AD-A035 694 TEXAS UNIV AT AUSTIN APPLIED RESEARCH LABS F/G 20/1
SATURATION OF PLANE ACOUSTIC WAVES AND NOTES ON THE PROPAGATION--ETC(U)
JAN 77 D A WEBSTER F44620-76-C-0040
UNCLASSIFIED ARL-TR-77-4 AFOSR-TR-77-0065 NL

1 OF 2
AD A035694

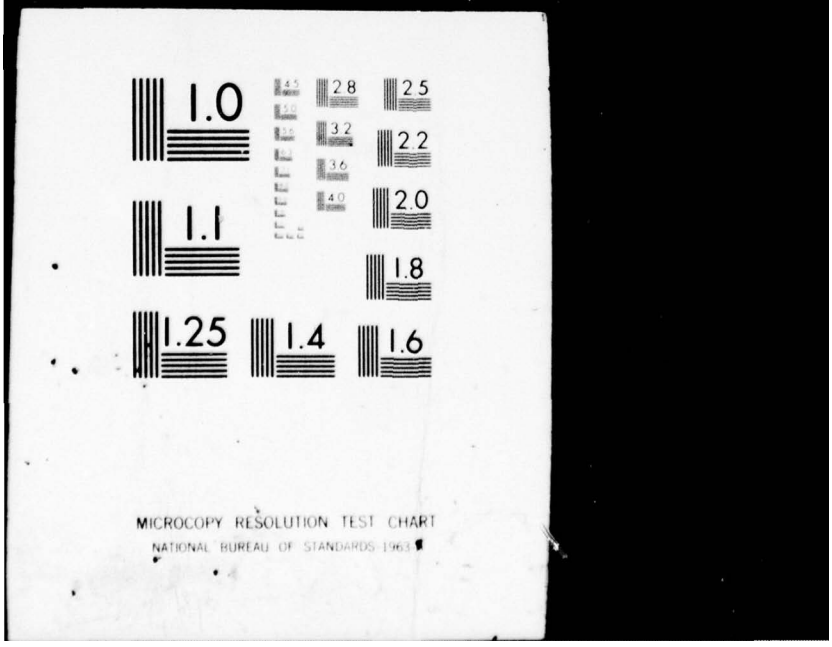
1.0
1.1
1.25
1.4
1.6
2.8
2.5
3.2
2.2
3.6
2.0
4.0
1.8
MICROCOPY RESOLUTION TEST CHART
NATIONAL BUREAU OF STANDARDS 1963

(12)

APPLIED RESEARCH LABORATORIES

THE UNIVERSITY OF TEXAS
AUSTIN

ARL-TR-77-4
January 1977

Copy No.

SATURATION OF PLANE ACOUSTIC WAVES AND NOTES ON THE PROPAGATION OF FINITE-AMPLITUDE SPHERICAL WAVES

NATIONAL OCEANIC AND ATMOSPHERIC ADMINISTRATION
Grant 04-5-022-12
AIR FORCE OFFICE OF SCIENTIFIC RESEARCH
Contract F44620-76-C-0040
NATIONAL AERONAUTICS AND SPACE ADMINISTRATION
Contract NASI-14160

Don A. Webster

AIR FORCE OFFICE OF SCIENTIFIC RESEARCH (AFSC)
NOTICE OF TRANSMITTAL TO DDC
This technical report has been reviewed and is approved for public release IAW AFR 190-12 (7b).
Distribution is unlimited.
A. D. BLOSE
Technical Information Officer

SECURITY CLASSIFICATION OF THIS PAGE (When Data Entered)

REPORT DOCUMENTATION PAGE	READ INSTRUCTIONS BEFORE COMPLETING FORM
1. REPORT NUMBER: AFOSR - TR - 77 - 0065	2. GOVT ACCESSION NO. / 3. RECIPIENT'S CATALOG NUMBER
4. TITLE (and Subtitle): SATURATION OF PLANE ACOUSTIC WAVES AND NOTES ON THE PROPAGATION OF FINITE-AMPLITUDE SPHERICAL WAVES	5. TYPE OF REPORT & PERIOD COVERED: INTERIM
	6. PERFORMING ORG. REPORT NUMBER
7. AUTHOR(s): DON A WEBSTER	8. CONTRACT OR GRANT NUMBER(s): F44620-76-C-0040
9. PERFORMING ORGANIZATION NAME AND ADDRESS: THE UNIVERSITY OF TEXAS AT AUSTIN APPLIED RESEARCH LABORATORIES AUSTIN, TEXAS 78712	10. PROGRAM ELEMENT, PROJECT, TASK AREA & WORK UNIT NUMBERS: 681307 9781-02 61102F
11. CONTROLLING OFFICE NAME AND ADDRESS: AIR FORCE OFFICE OF SCIENTIFIC SESEARCH/NA BLDG 410 BOLLING AIR FORCE BASE, D C 20332	12. REPORT DATE: Jan 77 13. NUMBER OF PAGES: 99
14. MONITORING AGENCY NAME & ADDRESS(if different from Controlling Office)	15. SECURITY CLASS. (of this report): UNCLASSIFIED 15a. DECLASSIFICATION DOWNGRADING SCHEDULE

16. DISTRIBUTION STATEMENT (of this Report)

Approved for public release; distribution unlimited.

17. DISTRIBUTION STATEMENT (of the abstract entered in Block 20, if different from Report)

18. SUPPLEMENTARY NOTES

19. KEY WORDS (Continue on reverse side if necessary and identify by block number)

NOISE
FINITE AMPLITUDE SPHERICAL WAVES
NON-LINEAR ACOUSTICS
SATURATION OF PLANE ACOUSTIC WAVES

20. ABSTRACT (Continue on reverse side if necessary and identify by block number)

The saturation of plane acoustic waves in an air-filled tube is investigated. Saturation, which is a state in which the signal amplitude at a field point approaches a limiting value, independent of source amplitude, is caused by non-linear propagation distortion. We observed it in a 30 m long, 5 cm i.d. progressive wave tube. Measured saturation curves were obtained for the following source conditions: sound pressure levels from 110 to 163 dB, frequencies from 500 Hz to 3500 Hz. The model equations of Merklinger and Rudnick were adapted and solved to give theoretical predictions for the fundamental component of the

DD FORM 1 JAN 73 1473 EDITION OF 1 NOV 65 IS OBSOLETE

UNCLASSIFIED
SECURITY CLASSIFICATION OF THIS PAGE (When Data Entered)

wave. The Merklinger model is found to give good results at low levels, and the Rudnick model at high levels. The measurement generally confirm the theoretical predictions. Dispersion due to the tube wall boundary layer is not included in either of the theoretical models. Its effect was analyzed separately and found to be not great for the fundamental component. Certain aspects of the propagation of spherically spreading waves of finite amplitude were also studied. A graphical method for assessing the importance of nonlinearity on spherical waves is discussed. New theoretical results for weak waves and for strong waves were found. In the first case a high order perturbation solution of Burgers' equation was obtained. In the second, the Rudnick model equation for the fundamental component of a sawtooth spherical wave was solved. In both cases, measurements taken in two outdoor propagation experiments confirmed the theoretical results.

(14) ARL-TR-77-4
January 1977

(6) SATURATION OF PLANE ACOUSTIC WAVES AND NOTES ON THE PROPAGATION OF FINITE-AMPLITUDE SPHERICAL WAVES.

(9) Interim rept.,

(10) Don A. Webster

(11) Jan 77 (12) 100 p.

(15) NATIONAL OCEANIC AND ATMOSPHERIC ADMINISTRATION
Grant 04-5-022-12
AIR FORCE OFFICE OF SCIENTIFIC RESEARCH
Contract F44620-76-C-0040
NATIONAL AERONAUTICS AND SPACE ADMINISTRATION
Contract NASI-14169

(16) 9781 (17) 02

(18) AFOSR

(19) TR-77-0065

APPLIED RESEARCH LABORATORIES
THE UNIVERSITY OF TEXAS AT AUSTIN
AUSTIN, TEXAS 78712

1473

404 434 LB

FOREWORD

This report is an adaptation of Don A. Webster's thesis, "Saturation of Plane Acoustic Waves and Notes on the Propagation of Finite-Amplitude Spherical Waves," which was written for the degree of Master of Science in Engineering at The University of Texas at Austin. Mr. Webster was enrolled in the Department of Electrical Engineering, and his degree was granted in December 1976.

The research was carried out at the Applied Research Laboratories and was supported by the Air Force Office of Scientific Research under Contract F44620-76-C-0040, by the National Aeronautics and Space Administration under Contract NAS1-14160, and by the National Oceanic and Atmospheric Administration under Grant 04-5-022-12. Technical monitors were Lt. Col. R. C. Smith and Lt. Col. L. W. Ormand for AFOSR, Dr. J. M. Seiner for NASA, and Dr. F. F. Hall for NOAA.

Readers particularly interested in the outdoor propagation measurements reported briefly in Appendices B and C may wish to consult Mark A. Theobald's thesis, "Experimental Study of Outdoor Propagation of Spherically Spreading Periodic Acoustic Waves of Finite Amplitude." This thesis, which is Ref. 28 in the present work, is soon to be issued as Applied Research Laboratories Technical Report ARL-TR-77-5 (January 1977) and subsequently, in somewhat different form, as a NASA Contractor Report. Experimental details as well as several additional outdoor experiments are given in Theobald's thesis.

David T. Blackstock
Supervisor

ABSTRACT

This paper investigates the saturation of plane acoustic waves in an air-filled tube. Saturation, a state in which the signal amplitude at a field point approaches a limiting value, independent of source amplitude, is caused by nonlinear propagation distortion. The author observed it in a 30-m long, 5-cm i.d. progressive wave tube. Measured saturation curves were obtained for the following source conditions: sound pressure levels from 110 to 163 dB, frequencies from 500 Hz to 3500 Hz. The model equations of Merklinger and Rudnick were adapted and solved to give theoretical predictions for the fundamental component of the wave. The Merklinger model is found to give good results at low levels, and the Rudnick model at high levels. The measurements generally confirm the theoretical predictions. The effect of dispersion due to the tube wall boundary layer, is not included in either of the theoretical models. Its effect was analyzed separately and found to be not great for the fundamental component.

Certain aspects of the propagation of spherically spreading waves of finite amplitude were also studied. A graphical method for assessing the importance of nonlinearity on spherical waves is discussed. New theoretical results for weak waves and for strong waves were found. In the first case a high order perturbation solution of Burgers' equation was obtained. In the second, the Rudnick model equation for the fundamental component of a sawtooth spherical wave was solved. In both cases, measurements taken in two outdoor propagation experiments confirmed the theoretical results.

TABLE OF CONTENTS

LIST OF FIGURES

GLOSSARY OF IMPORTANT SYMBOLS

a	tube internal radius
B_n	normalized particle velocity amplitude of the nth harmonic component corrected for spherical spreading $\left(= \frac{r}{r_o} \frac{u_n}{u_{10}}\right)$
c_o	small-signal sound speed
f	frequency
k	wavenumber $\left(= \frac{\omega}{c_o}\right)$
p	acoustic pressure
p_n	pressure amplitude of the nth harmonic component
p_{no}	pressure amplitude of the nth harmonic component at x=0
P_p	peak pressure amplitude of a sawtooth wave
P_r	Prandtl number
r	range (spherical waves)
$\bar{r}$, $\hat{r}$	shock and sawtooth formation distances (spherical waves)
r_{max}	range at which the rates of finite-amplitude and small-signal attenuation are equal (spherical waves)
r_o	a reference distance
t	time
t'	retarded time $\left(= t - \frac{x}{c_o}\right.$ for plane waves, $= t - \left(\frac{r-r_o}{c_o}\right)$ for spherical waves)
u_n	particle velocity amplitude of the nth harmonic component
u_{no}	particle velocity amplitude of the nth harmonic component at x=0
$V^{(n)}$	normalized nth order perturbation solution of Burgers' equation corrected for spherical spreading $\left(= \frac{r}{r_o} \frac{u^{(n)}}{u_{10}}\right)$
x	distance (plane waves)

$\bar{x}$, $\hat{x}$	shock and sawtooth formation distances (plane waves)
x_{max}	distance at which the rates of finite-amplitude and small-signal attenuation are equal (plane waves)
y	phase ($= \omega t'$)
α	absorption coefficient at angular frequency ω
α_n	absorption coefficient at angular frequency $n\omega$
β	parameter of nonlinearity $\left(= \frac{\gamma + 1}{2} \text{ for air}\right)$
γ	ratio of specific heats
Δ	boundary layer thickness $\left(= \left(\frac{2\nu}{\omega}\right)^{1/2}\right)$
ϵ	the acoustic Mach number $\left(= \frac{p_{10}}{\rho_o c_o^2}\right)$
λ	wavelength
ν	kinematic viscosity
ρ_o	ambient density
σ	dimensionless distance ($= \beta\epsilon k x$ for plane waves, $= \beta\epsilon k r_o \ln\left(\frac{r}{r_o}\right)$ for spherical waves)
σ_o	a dimensionless reference distance ($= \beta\epsilon k r_o$)
φ	a phase angle
ω	the angular frequency

CHAPTER 1

INTRODUCTION

In linear acoustic theory the amplitude of the received signal at a fixed point varies in direct proportion to the source amplitude. As the source amplitude is increased, however, losses due to finite amplitude effects develop. The received level increases less rapidly than the source level. Eventually the finite amplitude losses, or extra attenuation,* become so severe that the received signal approaches an upper limit, independent of source amplitude. The wave is said to have saturated.

The terminology used to describe the development of acoustic saturation may be made clear by Fig. 1-1. What is plotted here is the received sound pressure level (SPL) at a fixed distance versus the source SPL. Such a plot is commonly referred to as an amplitude response or input-output curve. At sufficiently low source levels the wave propagates as a small signal and the input-output curve (solid curve) has unit slope. Eventually the curve begins to bend over and depart from the extrapolated small-signal curve (dashed line), signifying that the approach to saturation has begun. The extra attenuation in decibels, commonly called EXDB, is the difference between the extrapolated small-signal curve and the input-output curve. The saturation level is the asymptotic value of the received level in the limit of high source levels. In practice, of

*Extra attenuation here is defined as attenuation over and above that observed for a small-signal wave.

course, the asymptote can never be attained. It is therefore useful to define a point at which the received level differs from the saturation level by some prescribed amount (for example, 1 dB). This point defines the beginning of the plateau region, where the input-output curve is nearly horizontal. In this region the wave is practically saturated.

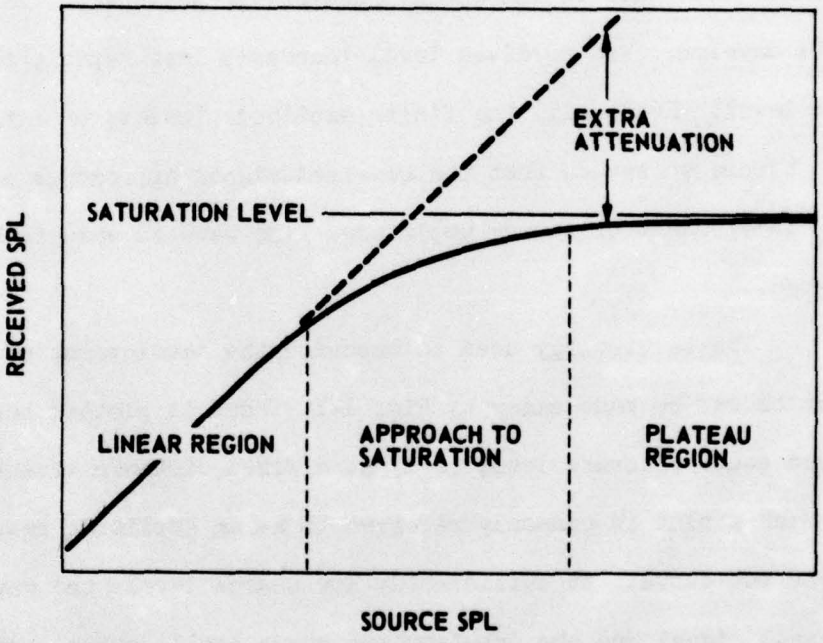

FIGURE 1-1
THE DEVELOPMENT OF SATURATION

The extra attenuation, which is responsible for saturation, is caused by a transfer of the wave's energy to higher frequency components where it is more efficiently dissipated. The energy transfer may be traced to the dependence of the propagation speed dx/dt of the wave on the local particle velocity u. The propagation speed of a particular wavelet (hence a particular value of u) is[1]

$$\left.\frac{dx}{dt}\right|_{u=\text{constant}} = c_o + \beta u \quad . \qquad (1\text{-}1)$$

Here c_o is the small-signal sound speed and β is the parameter of nonlinearity ($\beta=(\gamma+1)/2$ for gases, where γ is the ratio of specific heats). The dependence of dx/dt on u is a consequence of two phenomena. First, since sound propagates longitudinally, the wave is carried along by the motion of the medium (i.e., the sound wave is convected). Second, because of the nonlinearity of the pressure-density relation, wavelets associated with the compression phase of the wave travel faster than wavelets associated with the rarefaction phase. These two effects reinforce each other and cause a cumulative distortion of the wave as it propagates. For example, in the absence of ordinary dissipation, a sinusoidal wave will distort into a sawtooth wave. The harmonic distortion necessary to produce the sawtooth comes at the expense of the fundamental component. In other words, energy transfer takes place.

Most of the work that has been done on acoustic saturation concerns spherically spreading sound waves. Allen,[2] who made measurements on spherical waves in air, reported the first experimental evidence of acoustic saturation in 1950. Allen's measurements of the first six harmonics of the received signal show a definite approach to saturation. At a distance of 2 m from the source Allen found that an increase in source SPL* from 158 dB to 161 dB yielded only a 0.5 dB increase in the received level. An experiment on saturation of spherical waves in water is given in Ref. 3; this reference also contains an excellent historical review of other work relating to acoustic saturation of spherical waves.

*In the remainder of this work unless otherwise noted the SPL reference pressure is 0.0002 μbar.

Little experimental work has been done on saturation of plane waves. Plane waves are usually achieved either by generating a collimated beam in an open medium or by confining the sound wave in a tube. Lester[4] made measurements on a collimated ultrasonic beam in water. His measurements confirm the plateau region shown in Fig. 1-1 though the plateau turns down unexpectedly at the highest amplitudes.[3] Although much work on plane finite-amplitude waves has been done in tubes (see, for example, Refs. 5-9), a specific investigation of acoustic saturation has not been made. Pernet and Payne,[9] for example, made measurements of intense sound in tubes, but they, as many others, were primarily interested in the harmonic growth with distance and hence did not investigate saturation explicitly.

The object of this research is to investigate saturation of plane acoustic waves in tubes. Several model theories for the fundamental component of the wave are discussed. Solutions of the differential equations based on these models are compared with data taken in a plane wave tube in air. A numerical algorithm developed by Pestorius[8] to compute the wave shape at any propagation distance is also compared with data from the plane wave tube.

Although we have been mainly concerned in this research with plane waves, some new results have been obtained for spherical waves. These results are given in the appendices. In Appendix A a graphical method for assessing the importance of nonlinear effects on spherical waves is described. This method, which is a simplification of one described in Ref. 3, allows one to classify nonlinear effects as weak, moderate, or strong. A perturbation solution useful for weak waves is

presented in Appendix B. A solution valid for strong waves is presented in Appendix C. Both the weak and strong wave solutions are compared with data from freefield propagation experiments.

CHAPTER 2

REVIEW OF THE LITERATURE

A. Introduction

In this chapter we review several of the theoretical methods which may be applied to the problem of propagation of plane acoustic waves of finite amplitude. Our goal is to find an expression for the fundamental component of an initially sinusoidal wave. Both nonlinear effects and ordinary dissipation are taken into account. The specific problem we consider is the propagation of progressive waves contained in a gas-filled tube. The analysis in Section C of this chapter shows that for our experimental conditions only boundary layer absorption is important. We shall, however, in two cases present results valid only for a thermoviscous gas. These results are included because the methods used may, in some cases, be recast in terms of boundary layer absorption.

B. Review of Weak-Shock Theory

Because extensive use is made here of weak-shock theory, an outline of its basic features is appropriate. The exact one-dimensional equation for plane progressive waves in an ideal lossless gas is[1]

$$\frac{\partial u}{\partial t} + \left[c_o + \beta u\right] \frac{\partial u}{\partial x} = 0 \quad . \tag{2-1}$$

Given the boundary condition

$$u(0,t) = g(t) \quad , \tag{2-2a}$$

Poisson[10] found the solution (generalized here for an adiabatic gas) to be

$$u = g\left(t - \frac{x}{c_o + \beta u}\right) \quad . \tag{2-2b}$$

As Challis[11] later found, however, the Poisson solution leads to multivalued waveforms. The multivaluedness indicates the presence of shocks in the waveform.[1] To see this consider the propagation speed of a given wavelet (Eq. 1-1). Applying Eq. 1-1 to the wave pulse in Fig. 2-1 we see that point b will catch up to point a, ($x=x_1$), and eventually pass it, ($x=x_2$). The multivaluedness comes about because we have ignored dissipation up to this point. At high waveform gradients (such as those occurring at a shock, for example), dissipation is of paramount importance. Dissipation prevents the wave from folding over on itself.

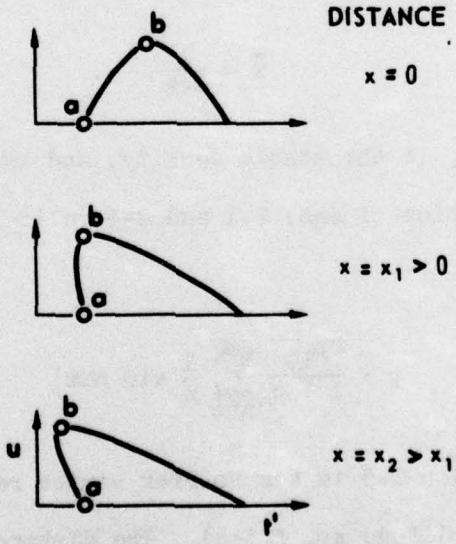

FIGURE 2-1
PROPAGATION OF A PULSE WHEN Eq. 1-1 IS APPLIED
[HERE $t' = t - \frac{x}{c_o}$ IS THE RETARDED TIME]

An extension of the Poisson solution (Eq. 2-3), weak-shock theory enables us to calculate the wave shape when shocks are present. Through the use of the Rankine-Hugoniot shock relations, which state conservation laws, shock dissipation is included. An excellent account of weak-shock theory is given by Blackstock.[12] We give here a brief account of the solution corresponding to a sawtooth wave shape. The inclusion of this solution is essential here, since it is the formation of the sawtooth wave shape which ultimately leads to saturation. We consider a source excitation of the form

$$p(0,t) = p_{10} \sin \omega t \quad . \tag{2-3}$$

Here p, ω, and p_{10} are the acoustic pressure, angular frequency, and pressure amplitude, respectively, of the source. A discontinuity in the wave (a shock) is first formed at a distance $\bar{x}$ given by[12]

$$\bar{x} = \frac{1}{\beta \epsilon k} \quad . \tag{2-4}$$

Here $\epsilon = p_{10}/\rho_o c_o^2$, ρ_o is the static density, and $k = \omega/c_o$ is the wave number. An approximate solution of Eqs. 2-1 and 2-3 valid in the more remote region $x > 3\bar{x}$ is[12]

$$p = \frac{2p_{10}}{1+\sigma} \sum_{n=1}^{\infty} \frac{1}{n} \sin n\omega t' \quad , \tag{2-5}$$

where $\sigma = x/\bar{x}$. Equation 2-5 is the Fourier series representation for a sawtooth wave of amplitude $\pi p_{10}/(1+\sigma)$. The distance $x = 3\bar{x}$ ($\sigma = 3$) is commonly called the sawtooth distance, and the region of validity of Eq. 2-5 is called the sawtooth region.

As will be shown in Chapter 3, Section B, Eq. 2-5 may be used to indicate the development of saturation. In many cases, however, ordinary absorption must also be taken into account. In the following section we examine the role of ordinary absorption and dispersion in our experiments.

C. The Role of Ordinary Absorption and Dispersion

Ordinary absorption may be expected to be important in our measurements. Indeed, Pestorius[8] found it necessary to include both absorption and dispersion in his analysis of finite-amplitude propagation in tubes. Some of the effects of absorption and dispersion on a small-signal wave are discussed here so that the role of each in the nonlinear case may be better understood.

The problem of absorption and dispersion of plane sound waves in tubes was first solved by Kirchhoff.[13] For a wide tube* one finds that the absorption coefficient α and phase velocity c_{ph} are given by

$$\alpha = \frac{1}{a}\sqrt{\frac{\omega\nu}{2c_o^2}}\left[1 + \frac{\gamma - 1}{\sqrt{Pr}}\right] , \qquad (2\text{-}6)$$

and

$$c_{ph} = \frac{c_o}{1 + c_o\alpha/\omega} . \qquad (2\text{-}7)$$

*A wide tube is a tube for which the boundary layer thickness Δ[14] is small compared to a. We define the boundary layer thickness Δ as the distance from the tube wall to the point where the particle velocity amplitude has reached a value equal to 1/e times its mainstream value. It turns out that $\Delta = \sqrt{2\gamma/\omega}$. The requirement $\Delta \ll a$ thus imposes a lower limit on the frequencies for which the wide tube formulas may be used. The tube must not, however, be so wide that losses in the fluid mainstream are comparable to the boundary layer losses. The latter requirement may be stated as $a \ll 1/k^2\Delta$.[15] Hence a wide tube must meet the requirement that $\Delta \ll a \ll 1/k^2\Delta$. For example, to be classified wide over the frequency region 100 Hz to 30 kHz, the tube must have a radius in the range 0.02 cm $\ll$ a $\ll$ 30 cm. The pipe we use for our experiments (see Chapter 4) has a radius of 2.5 cm. Our pipe, therefore, is a wide pipe from 100 Hz to 30 kHz.

Here a is the tube radius, ν is the kinematic viscosity, and Pr is the Prandtl number. From Eqs. 2-6 and 2-7 we see that c_{ph} decreases with frequency, asymptotically approaching c_o in the high frequency limit. The absorption coefficient α varies as the square root of ω. From these observations we conclude that a nonsinusoidal signal propagating in a tube will suffer both phase and amplitude distortion.

The importance of ordinary absorption in our experiments is easily seen from Eq. 2-6. The tube we use for our measurements has a 2.5 cm radius, and the (fundamental) frequency range of interest is 500 Hz to 4000 Hz. At a frequency of 3.5 kHz, for example, the absorption coefficient α is about 0.072 Np/m. Therefore, for the available measurement distance, 26 m, we could expect 16.3 dB of small-signal attenuation alone. We conclude that a reasonable theory for our experiments must include the effect of ordinary absorption.

The importance of dispersion may be seen from an examination of the phase distortion suffered by a nonsinusoidal signal. Since we are concerned with saturation in our experimental work, the main waveform of interest besides the sine wave is the sawtooth. McKittrick et al.[16] were able to explain asymmetric waveforms observed in a high intensity tube experiment by considering the propagation of a small-signal sawtooth wave. We present an analysis similar to theirs here because it makes clear the effect of absorption and dispersion on the overall wave shape. We assume a sawtooth wave of peak-to-peak amplitude p_o exists at x=0. The normalized acoustic pressure p/p_o may then be expressed as the Fourier series

$$\left(p/p_o\right)_{x=0} = \frac{2}{\pi} \sum_{n=1}^{\infty} \frac{1}{n} \sin n\omega t \quad . \tag{2-8}$$

If Eqs. 2-6 and 2-7 are applied, p/p_o is given at distance x by[16]

$$p/p_o = \frac{2}{\pi} \sum_{n=1}^{\infty} \frac{e^{-\sqrt{n}\alpha x}}{n} \sin n\left(\omega t' - \sqrt{n}\alpha x\right) \quad . \tag{2-9}$$

Figure 2-2 shows the sum of the first one hundred terms of Eq. 2-9 for three cases. The top waveform is one in which there is no absorption or dispersion, i.e., αx has been set to zero. Note the Gibbs' overshoot at both peak and trough. For the middle and bottom waveforms the value of αx is 0.3. In the middle waveform absorption is included but not dispersion, i.e., the phase angles $\sqrt{n}\alpha x$ are ignored. The result is that the waveform is rounded symmetrically at both peak and trough. In the bottom waveform both absorption and dispersion are included. The wave asymmetry is clear; the peak is rounded while the trough remains sharp.

We now ask what effect dispersion will have on a wave of finite-amplitude. Dispersion clearly alters the wave shape in the linear case and, as McKittrick et al. found, causes the waveforms to be asymmetric in the finite-amplitude case as well. What we are mainly concerned with, however, are the harmonic amplitudes. For a small-signal wave, dispersion does not alter the harmonic amplitudes, i.e., the spectra of the middle and bottom waveforms in Fig. 2-1 are identical. The propagation of a finite-amplitude wave, however, is highly dependent upon the wave shape.[8] Consider, for example, the propagation of two waves, one a sawtooth and the other an inverted sawtooth. Although both have the same initial spectra, the finite-amplitude distortion of the two waves is vastly different. The reason is that the phases of the Fourier components, and therefore the wave shapes, are different. This is admittedly a rather

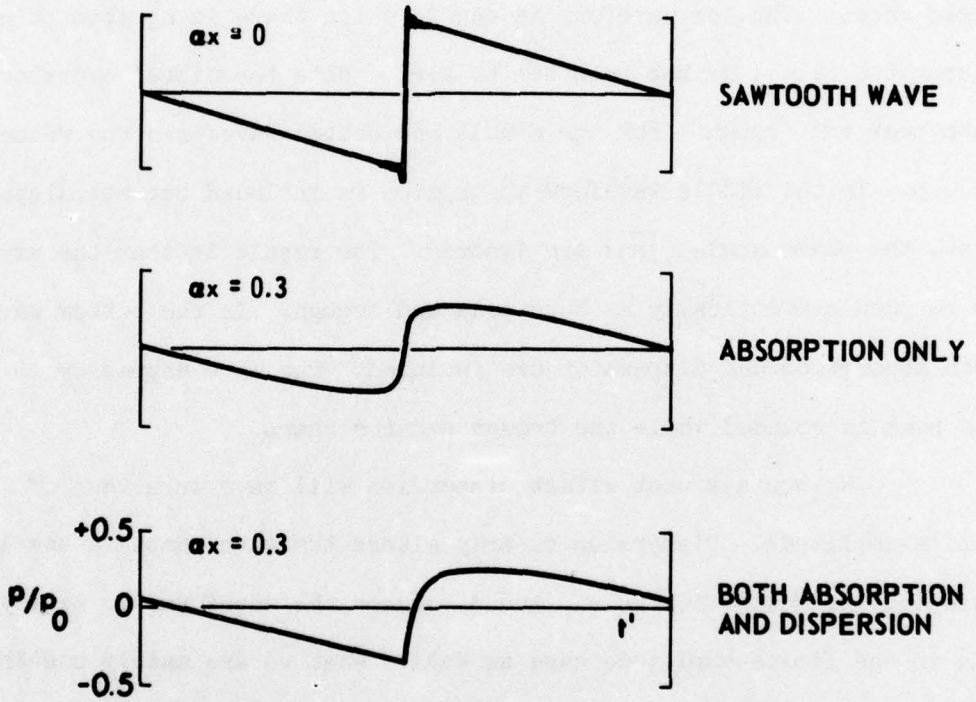

FIGURE 2-2
EFFECTS OF ABSORPTION AND DISPERSION
ON A SMALL-SIGNAL WAVE

drastic example, given merely to point out that dispersion will probably have some effect on the propagation of the wave. A qualitative discussion of the effect of dispersion is given in Chapter 6. The discussion given there is based on the bottom waveform of Fig. 2-2.

The effects of both dispersion and ordinary absorption are usually included in a theoretical analysis in one of two ways, both of which are treated briefly in Section D. In the first method the effects are included as specific terms in the differential or integral equation governing the wave motion. Unfortunately, however, the equation is generally very difficult to solve. Another method is to include the effects stepwise in a computer algorithm that is based on a mathematical model of the wave distortion process. Such an algorithm has been described by Pestorius.[8] Although the algorithm is not efficient for computing saturation curves, we do make use of it in Chapter 6. There a quantitative discussion of the effects of dispersion are given.

A completely different approach is to ignore dispersion entirely. Several ad hoc models have been proposed in which ordinary absorption is accounted for but not dispersion. Perhaps surprisingly, several of these models have enjoyed considerable success. Appropriate ones are discussed in Section D.

D. Contributions of Other Researchers

1. A Computational Method - Pestorius' Algorithm

In a computer algorithm developed by Pestorius, explicit account is taken of nonlinear effects, ordinary absorption, and dispersion.[8] In this algorithm the source wave is "computer propagated" a short distance

Δx; the basis of the computation is weak-shock theory. The resulting time waveform is then transformed to the frequency domain, where corrections are made for small-signal absorption and dispersion. After a transfer back to the time domain, another short propagation step is made. In this way the time waveform may be computed for any propagation distance. The validity of this algorithm has been verified by Pestorius for both initially sinusoidal waves and noise.[8] As was mentioned in Section C, we make use of this algorithm in Chapter 6 to find the effect of dispersion on the harmonic amplitudes. The algorithm was not, however, used to compute amplitude response curves because a separate computer run would have been required for each increment in source SPL.

2. Burgers' Equation

a. Mainstream Absorption

Lighthill[17] reduced the equations of motion for progressive plane waves in an unbounded thermoviscous gas by a series of approximations to Burgers' equation. Mendousse[18] cast Burgers' equation in the following form, which is equally valid but better suited for boundary value problems:

$$\frac{\partial u}{\partial x} - \frac{\beta}{c_o^2} u \frac{\partial u}{\partial t'} = \frac{\alpha}{\omega^2} \frac{\partial^2 u}{\partial t'^2} \quad , \tag{2-10}$$

where α is the thermoviscous absorption coefficient at angular frequency ω.[15] It will be seen that the left-hand side of Eq. 2-10 is an approximate form of Eq. 2-1. The right-hand side is the dissipation term appropriate for mainstream absorption. Though exact solutions of Eq. 2-10 are known, they are not relevant for our problem because in our case the

attenuation is due to boundary layer effects, not mainstream effects. The spherical wave version of Eq. 2-10 is, however, treated in Appendix B by a perturbation method.

b. Boundary Layer Absorption

Blackstock[1] found a "Burgers-like" equation for finite-amplitude waves subject to boundary layer attenuation,

$$\frac{\partial u}{\partial x} - \frac{\beta}{c_o^2} u \frac{\partial u}{\partial t'} = \alpha \sqrt{\frac{2}{\pi\omega}} \int_o^\infty \frac{\partial u(x,t'-\lambda)}{\partial t'} \frac{d\lambda}{\sqrt{\lambda}} \quad . \qquad (2\text{-}11)$$

Here α is the boundary layer absorption coefficient at angular frequency ω; see Eq. 2-6. Solutions of Eq. 2-11 would be ideal for our work. Unfortunately, however, only low-order perturbation solutions have been found and they are not applicable in our study.[19] Evaluation of Eq. 2-11 by numerical means was not pursued. Coppens and Sanders[20] also found a "Burgers-like" equation for tubes. Their equation is, however, less general than Eq. 2-11 in that it is limited to periodic waves.

3. Ad Hoc Models

A great body of the literature regarding plane propagation of finite-amplitude waves in a lossy medium is devoted to the subject of ad hoc models. The models presented here illustrate some of the methods of blending nonlinear effects and ordinary dissipation. No one has yet, unfortunately, found a way to include the effects of dispersion.

a. Merklinger's Method

Merklinger[21] applied Westervelt's equation[22]

$$\frac{dI_1}{dx} = - 2\alpha_1 I_1 - \langle p(x,t')q(x,t') \rangle \qquad (2\text{-}12)$$

to the problem of plane wave propagation in a viscous fluid. Here I_1 is the intensity of the fundamental frequency component at distance x, and α_1 is the absorption coefficient (appropriate for a viscous fluid) at the fundamental frequency. The angled brackets indicate a time average over one period of the wave, and q is the source function given by

$$q(x,t) = \frac{\beta}{\rho_o^2 c_o^4} \frac{\partial}{\partial t} \left[p(x,t) \right]^2 \quad . \qquad (2\text{-}13)$$

Merklinger assumed that the nonlinear decay of the fundamental pressure component $p_1(x,t')$ is primarily due to work that it does on the second harmonic pressure component $p_2(x,t')$. That is, Merklinger approximated p as*

$$p \doteq p_1(x,t') + p_2(x,t') \quad . \qquad (2\text{-}14)$$

For $p_2(x,t')$, Merklinger used a second order perturbation solution[9] of the nonlinear wave equation for a viscous fluid. The boundary condition is given by Eq. 2-3.

$$p_2(x,t') = \frac{p_{10}^2 \beta \omega}{4\rho_o c_o^3} \left[\frac{e^{-2\alpha_1 x} - e^{-4\alpha_1 x}}{\alpha_1} \right] \sin 2\omega t' \qquad (2\text{-}15)$$

*We here define p_n to be the pressure amplitude of the nth harmonic. If the time dependence is to be included, we shall use the form $p_n(x,t')$.

Writing $p_1(x,t')$ as

$$p_1(x,t') = p_1(x) \sin \omega t' \quad , \tag{2-16}$$

and reinterpreting $p_{10}^2 e^{-2\alpha_1 x}$ in Eq. 2-15 as $p_1^2(x)$, we may write $p_2(x,t')$ as

$$p_2(x,t') = p_1^2(x) \frac{\beta\omega}{4\rho_o c_o^3 \alpha_1} \left(1 - e^{-2\alpha_1 x}\right) \sin 2\omega t' \quad . \tag{2-17}$$

The differential equation for p_1 may be found from Eqs. 2-12 through 2-17. The result is

$$\frac{dp_1}{dx} = \alpha_1 p_1 - \frac{\beta k^2}{8\alpha_1 \rho_o^2 c_o^4} \left(1 - e^{-2\alpha_1 x}\right) p_1^3 \quad . \tag{2-18}$$

The solution of Eq. 2-18 consistent with the boundary condition $p_1(0)=p_{10}$ is

$$p_1 = \frac{p_{10} e^{-\alpha_1 x}}{\left[1 + \frac{\Gamma^2}{16}\left(1 - e^{-2\alpha_1 x}\right)^2\right]^{1/2}} \quad , \tag{2-19}$$

where $\Gamma=1/\alpha_1\bar{x}$. The assumptions inherent in Eqs. 2-14 and 2-15 should be expected to limit the validity of Eq. 2-19. This problem is addressed in Chapter 3, Section B. We note in passing that Merklinger has found Eq. 2-19 to be in good agreement with an exact solution of Burgers' equation for a wide range of source amplitudes.[21]

In using Eq. 2-15 for $p_2(x,t')$ we have assumed a viscous fluid. To make use of Merklinger's method for the case of boundary layer absorption we must find an appropriate expression for $p_2(x,t')$. Thuras, Jenkins,

and O'Neil[23] derived an equation in which no assumption is made of a specific absorption mechanism. Their method is presented in the following section.

b. Method of Thuras, Jenkins, and O'Neil

Thuras et al. suggested an approximate method to take account of ordinary absorption in the initial growth of p_2. The basis for their method is the second order perturbation solution of Eq. 2-1,

$$p_2 = \frac{\beta k p_{10}^2 x}{2\rho_o c_o^2} \quad . \tag{2-20}$$

The spatial growth rate $(dp_2/dx)g$ is, from Eq. 2-20,

$$\left(\frac{dp_2}{dx}\right)_g = \frac{\beta k p_{10}^2}{2\rho_o c_o^2} \quad . \tag{2-21}$$

Thuras et al. reasoned that in the presence of absorption, p_{10} should be replaced by $p_{10}\exp(-\alpha_1 x)$ where α_1 is the absorption coefficient at the fundamental frequency. From this reasoning Eq. 2-21 becomes

$$\left(\frac{dp_2}{dx}\right)_g = \frac{\beta k p_{10}^2 e^{-2\alpha_1 x}}{2\rho_o c_o^2} \quad . \tag{2-22}$$

Thuras et al. reasoned that opposing the spatial growth rate represented by Eq. 2-22 was a spatial decay $(dp_2/dx)_d = -\alpha_2 p_2$ due to ordinary absorption. Here α_2 is the absorption coefficient at the frequency of the second harmonic. The total growth rate dp_2/dx was taken to be

$$\frac{dp_2}{dx} = \left(\frac{dp_2}{dx}\right)_d + \left(\frac{dp_2}{dx}\right)_g$$

$$= -\alpha_2 p_2 + \frac{\beta k p_{10}^2 e^{-2\alpha_1 x}}{2\rho_o c_o^2} \quad . \tag{2-23}$$

The solution of Eq. 2-23 which satisfies $p_2=0$ at $x=0$ is

$$p_2 = p_{10}^2 e^{-2\alpha_1 x} \frac{\beta k}{2\rho_o c_o^2} \left[\frac{1 - e^{-(\alpha_2 - 2\alpha_1)x}}{\alpha_2 - 2\alpha_1}\right] \quad . \tag{2-24}$$

In Chapter 3, Section B, we shall make use of Eq. 2-24 for the expression for p_2 required by Merklinger's model. It is interesting to note that if we set $\alpha_2=4\alpha_1$ (as would be the case for a viscous fluid) Eq. 2-15 results.

c. Rudnick Model

Rudnick[24] proposed a model for describing the decay of sawtooth waves in a tube. He assumed that the total decay rate of the peak pressure P_p is the sum of the decay rate due to small-signal absorption and the decay rate due to nonlinear effects (found from Eq. 2-5). Thus his model is similar to Thuras, Jenkins, and O'Neil's for p_2. Rudnick obtained

$$\frac{dP_p}{dx} = -\alpha_o P_p - \frac{\beta k}{\pi \rho_o c_o^2} P_p^2 \quad , \tag{2-25}$$

where α_o is a "zero order" coefficient for the tube wall attenuation of the wave.[24] The solution of Eq. 2-25 consistent with $P_p=P_p(0)$ at $x=0$ is

$$P_p = \frac{P_p(0)\, e^{-\alpha_o x}}{1 + \frac{\beta k P_p(0)}{\pi \alpha_o \rho_o c_o^2}\left(1 - e^{-\alpha_o x}\right)} \quad . \qquad (2\text{-}26)$$

A modified version of Eq. 2-25 is discussed in Chapter 3 as the theoretical model for the decay of the fundamental component of a sawtooth wave, and also in Appendix C for the spherical wave problem. Equation 2-25 is quite appealing physically and also yields simple solutions. As is always the case, however, the telling test is the experiment.

4. Summary

We have discussed several theoretical approaches that might be used in the description of saturation of plane waves in a tube. The Burgers' equation method, though certainly applicable, suffers from a lack of appropriate analytic solutions. The computational method of Pestorius, though appropriate, is not efficient for computing saturation curves. The ad hoc models do not include the effect of dispersion but they have yielded analytic solutions. The models pertain to the fundamental component p_1. Merklinger's model is based on an intensity equation, and Rudnick's model, on an amplitude equation. We shall use the ad hoc models for our theoretical models for p_1. The telling test of the models is, of course, the experiment.

CHAPTER 3

THEORETICAL DEVELOPMENT

A. Introduction

In this chapter the theoretical models used to describe the approach to saturation are presented. Attention is focused on the fundamental frequency component p_1 of the wave, though saturation is the ultimate fate of all the Fourier components. First, weak-shock theory is used to obtain formulas for saturation and the approach to saturation. We then endeavor to include the effects of tube wall dissipation. Although dispersion should be expected to play a role in determining the harmonic amplitudes, we have found no means to include it analytically. We do, however, make use of the algorithm of Pestorius to give an estimate of the effect of dispersion. This algorithm is not used to compute actual saturation levels because of the computation time required.

B. Estimates of the Approach to Saturation

1. Weak-Shock Theory

An estimate of the saturation amplitude may be found from weak-shock theory. The expression for the fundamental pressure p_1 in the sawtooth region is, from Eq. 2-5,

$$p_1 = \frac{2p_{10}}{1 + \sigma} \quad , \quad \sigma > 3 \quad . \tag{3-1}$$

The saturation amplitude p_{1sat}, found by letting the source amplitude p_{10} become large (i.e., $\sigma \gg 1$), is

$$p_{1sat} = \frac{2\rho_o c_o^2}{\beta k x} \quad . \tag{3-2}$$

Thus p_{1sat} is predicted to decrease with both frequency and distance. The inverse first power dependence of p_{1sat} on both frequency and distance is found only in cases where absorption over the entire waveform is unimportant. It is generally true, however, that the saturation level does decrease with increasing frequency and distance.

2. Merklinger's Model

As was mentioned in Chapter 2, Merklinger's model may be reinterpreted so that it applies to more than just viscous fluids. To do so, we make use of Thuras, Jenkins, and O'Neil's expression for the second harmonic pressure p_2 (Eq. 2-24). Substituting Eq. 2-24 for Eq. 2-15 and following the same analysis as in Chapter 2, Section 3.a., we find the differential equation for p_1 to be

$$\frac{dp_1}{dx} = -\alpha p_1 - \frac{\beta k^2}{4\rho_o^2 c_o^4}\left[\frac{1 - e^{-(\alpha_2 - 2\alpha_1)x}}{\alpha_2 - 2\alpha_1}\right] p_1^3 \quad . \tag{3-3}$$

The solution of Eq. 3-3 subject to the boundary condition $p_1(0)=p_{10}$ is simply

$$p_1 = \frac{p_{10}\, e^{-\alpha_1 x}}{\left(1 + \frac{\Gamma^2}{4\frac{\alpha_2}{\alpha_1}\left(\frac{\alpha_2}{2\alpha_1} - 1\right)}\left[\frac{\alpha_2}{2\alpha_1}\left(1 - e^{-2\alpha_1 x}\right) - \left(1 - e^{-\alpha_2 x}\right)\right]\right)^{1/2}} \quad . \tag{3-4}$$

If the small-signal attenuation is mainly due to tube wall effects,

$\alpha_2=\sqrt{2}\alpha_1$. Note that if $\alpha_2=4\alpha_1$, as would be the case for a viscous fluid, Eq. 3-4 reduces to Merklinger's result, Eq. 2-19.

What about the region of validity of Eq. 3-3? We should expect that use of the approximation $p\doteq p_1+p_2$ (Eq. 2-10) and the perturbation result for p_2 (Eq. 2-21) would limit the use of Eq. 3-4 to weak waves. Equation 3-4 seems to have wider validity, however. Let us examine, for example, the saturation level found from Eq. 3-4. The result is

$$p_{1sat} = \frac{2\rho_o c_o^2}{\beta k}\left[\frac{\frac{\alpha_2^2}{2} - \alpha_1\alpha_2}{\frac{\alpha_2}{\alpha_1}\left[1 - e^{-2\alpha_1 x}\right] - \left[1 - e^{-\alpha_2 x}\right]}\right]^{1/2} . \qquad (3\text{-}5)$$

Now let $\alpha_1,\alpha_2\to 0$. The weak-shock theory expression, Eq. 3-2, is recovered. We conclude that although several of the assumptions leading to Eq. 3-4 are not valid for strong waves, the saturation level is an appropriate strong-wave limit.

3. The Rudnick Model

We describe here a generalization of the method Rudnick used to obtain a formula for the peak amplitude of a sawtooth wave. The "Rudnick assumption" is that the decay rate of the fundamental pressure component dp_1/dx is the sum of the decay rate due to absorption $(dp_1/dx)_{abs.}=-\alpha_1 p_1$ and the decay rate $(dp_1/dx)_{f.a.}$ due to finite-amplitude effects. The latter decay rate is, from Eq. 3-1,

$$\left(\frac{dp_1}{dx}\right)_{f.a.} = -\frac{2\beta\epsilon k p_{10}}{(1+\sigma)^2} = -\frac{\beta\epsilon k}{2p_{10}}\,p_1^2 . \qquad (3\text{-}6)$$

The total decay rate dp_1/dx is then

$$\frac{dp_1}{dx} = \left(\frac{dp_1}{dx}\right)_{abs.} + \left(\frac{dp_1}{dx}\right)_{f.a.} = -\alpha_1 p_1 - \frac{\beta\epsilon k}{2p_{10}} p_1^2 \quad . \tag{3-7}$$

The solution of Eq. 3-7 is

$$p_1 = \frac{p_1(0)\, e^{-\alpha_1 x}}{1 + \frac{\beta k p_1(0)}{2\alpha_1 \rho_o c_o^2}\left(1 - e^{-\alpha_1 x}\right)} \quad , \tag{3-8}$$

where $p_1(0)$ is the fundamental pressure amplitude at x=0. If we require that Eq. 3-8 reduce to the weak-shock solution (Eq. 3-1) as $\alpha_1 \to 0$, then $p_1(0)$ must have the value

$$p_1(0) = 2p_{10} \quad . \tag{3-9}$$

This may seem a rather surprising result, since we have previously specified that the source amplitude is p_{10}, not $2p_{10}$. The discrepancy is only apparent, however, and not real. If we extrapolate the sawtooth solution (Eq. 2-5) back to x=0 we obtain,

$$p(0,t) = 2p_{10} \sum_{n=1}^{\infty} \frac{1}{n} \sin n\omega t \quad , \tag{3-10}$$

which represents a sawtooth wave of amplitude πp_{10}. This suggests that for distances $\sigma > 3$ the acoustic signal produced by a sine wave of amplitude p_{10} at x=0 is the same as that produced by a sawtooth wave whose fundamental has amplitude $2p_{10}$ at x=0. Clearly this will be the case only if absorption is not important over the initial propagation distance of three

shock formation lengths. We shall presently investigate the conditions under which this assumption is reasonable.

The equation for p_1 may be found by combining Eq. 3-8 and Eq. 3-9. The result is

$$p_1 = \frac{2p_{10}\, e^{-\alpha_1 x}}{1 + \dfrac{1 - e^{-\alpha_1 x}}{\alpha_1 \bar{x}}} \quad . \tag{3-11}$$

Again, as the source amplitude p_{10} increases (i.e., $\bar{x} \to 0$), the saturation amplitude p_{1sat} is obtained,

$$p_{1sat} = \frac{2\rho_o c_o^2 \alpha_1\, e^{-\alpha_1 x}}{\beta k\left(1 - e^{-\alpha_1 x}\right)} \quad . \tag{3-12}$$

It is seen that the saturation amplitude still decreases with increasing frequency and distance, though not in the same inverse relation given by the weak-shock formula, Eq. 3-2.

We now investigate the conditions under which the Rudnick model should be valid. In general, since the model equation, Eq. 3-7, is partially derived from the sawtooth solution, an inherent assumption is that the wave be strong enough to form a sawtooth. But when, in the presence of ordinary absorption, is sawtooth formation likely? (See Appendix A for a similar discussion for the spherical wave problem.) The shock and sawtooth formation distances in the absence of absorption may be easily computed for a given set of source and medium parameters. What is needed is an estimate of the distance x_{max} beyond which small-signal dissipation effects are more important than nonlinear dissipation effects.

Blackstock[12] computed the distance x_{max} at which the decay rates due to nonlinear effects (found from Eq. 3-1) and small-signal effects are equal. For plane waves the value of x_{max} is

$$x_{max} \doteq \frac{1}{\alpha} \quad . \tag{3-13}$$

The question of shock and sawtooth formation may thus be answered by analyzing the various possible relations between $\bar{x}$, $\hat{x}$, and x_{max}.[3] If the relation between x_{max} and $\bar{x}$ is

$$x_{max} < \bar{x} \quad , \tag{3-14}$$

shock formation is precluded. The high frequency components damp out before a shock can form. The inequality

$$\bar{x} < x_{max} < \hat{x} \tag{3-15}$$

indicates that shock formation is possible. Ordinary dissipation dominates, however, before a sawtooth can form. Sawtooth formation is likely if the relation is

$$\hat{x} < x_{max} \quad . \tag{3-16}$$

We see that the Rudnick model should be valid if Eq. 3-16 is satisfied. That is, Eq. 3-11 should be valid if $\hat{x}$ is less than $1/\alpha$.

CHAPTER 4

EXPERIMENTAL APPARATUS AND PROCEDURES

A. Introduction

In this chapter the equipment and procedures used in the experiments described in Chapter 5 are discussed. Individual equipment listings are given in Section B along with a general schematic of the experimental apparatus. In Section C the experimental procedures are discussed.

B. Experimental Apparatus

Figure 4-1 shows a generalized schematic of the experimental apparatus. The system has been used in several previous experiments (see, for example, Refs. 8 and 15). The microphone nearest the driver, called a source or monitor microphone, is used to measure the source waveform. This microphone also provides an input to an automatic gain control (AGC) circuit, which is used to stabilize the source SPL. The second microphone is the receiving microphone, which is variable in 3.7 m steps relative to the source microphone.

The experimental apparatus is divided into three systems: a transmitting system, the plane wave tube, and the receiving system. The specific pieces of equipment used in each of these systems are listed in the following three sections.

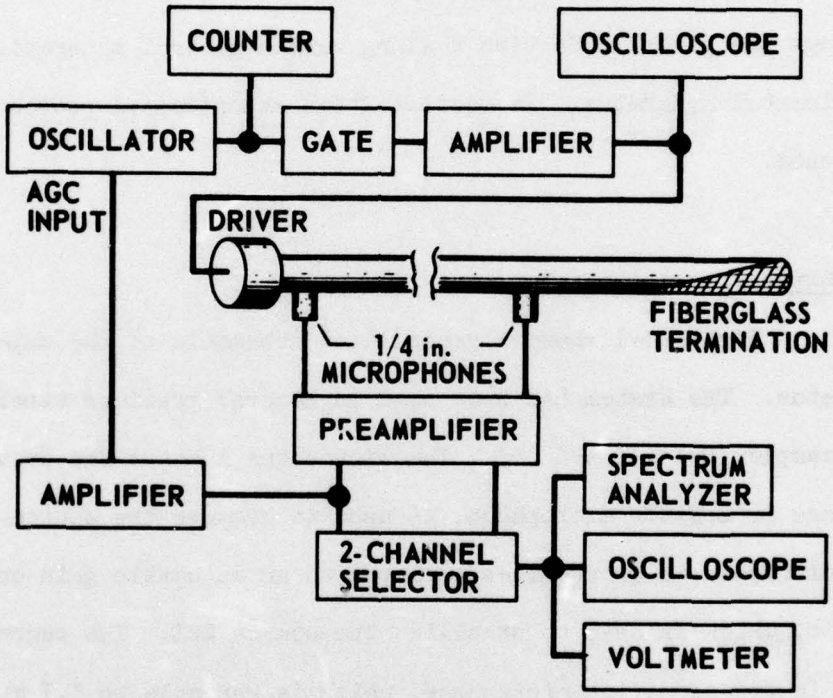

FIGURE 4-1
BLOCK DIAGRAM OF THE EXPERIMENTAL APPARATUS

1. The Transmitting System

The following pieces of equipment were used in the transmitting system.

(1) Oscillator. B&K type 1022 or H-P 3300A with 3302 A trigger/phase lock plug-in.

(2) Counter. H-P 5300 B.

(3) Gate. GR 1496.

(4) Amplifier. Altec model 250 B power amplifier.

(5) Oscilloscope. Tektronix 532.

(6) Driver. JBL model 375-H. This driver is commercially available with either a phenolic or aluminum diaphragm. Because of its much better high frequency response, the driver with the aluminum diaphragm was chosen for this experiment. A typical frequency response of one of the drivers is shown in Fig. 4-2. The response was taken

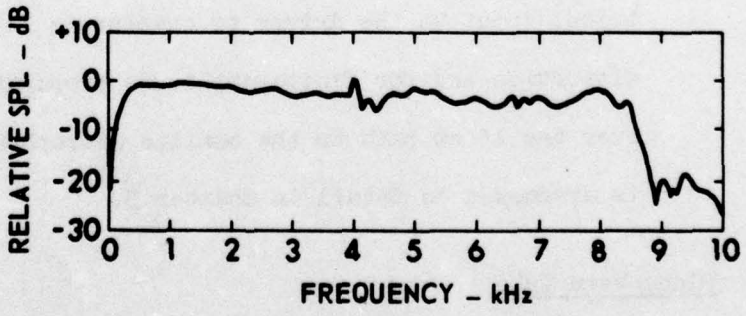

FIGURE 4-2
TYPICAL FREQUENCY RESPONSE
OF JBL 375-H DRIVER
(CONSTANT VOLTAGE INPUT)

with a constant voltage input to the driver. For this measurement the driver was coupled to the plane wave tube shown in Fig. 4-1. What is plotted in Fig. 4-2 is the relative SPL measured at the monitor microphone, which is approximately 13 cm from the driver throat. The response of the driver is flat within a 3 dB range from approximately 300 Hz to 8500 Hz. The maximum input power to the driver is specified as 30 Wrms. It was found, however, that driver failure occurred much less frequently when the input power was limited to 25 Wrms. At 25 Wrms input the maximum SPL at the monitor microphone was 157 dB at 500 Hz. To attain higher levels, provision was made for parallel operation of four 375-H drivers. The maximum SPL at the first microphone was then 163 dB at 500 Hz.

(7) Laboratory constructed predistortion network (not shown in Fig. 4-1). This network was used to predistort the electrical input to the driver to compensate for driver distortion and for finite-amplitude propagation distortion over the 13 cm path to the monitor microphone. The network is discussed in detail in Chapter 5.

2. Plane Wave Tube

The tube used in this experiment was originally constructed by McKittrick; see Ref. 16. It consists of eight 3.7 m sections of aluminum pipe joined by microphone-holding flanges. The pipe has a 2 m long fiberglass termination.[8] A typical flange assembly is shown in Fig. 4-3, taken from Ref. 15. The 1/4 in. microphone fits through the white teflon collar

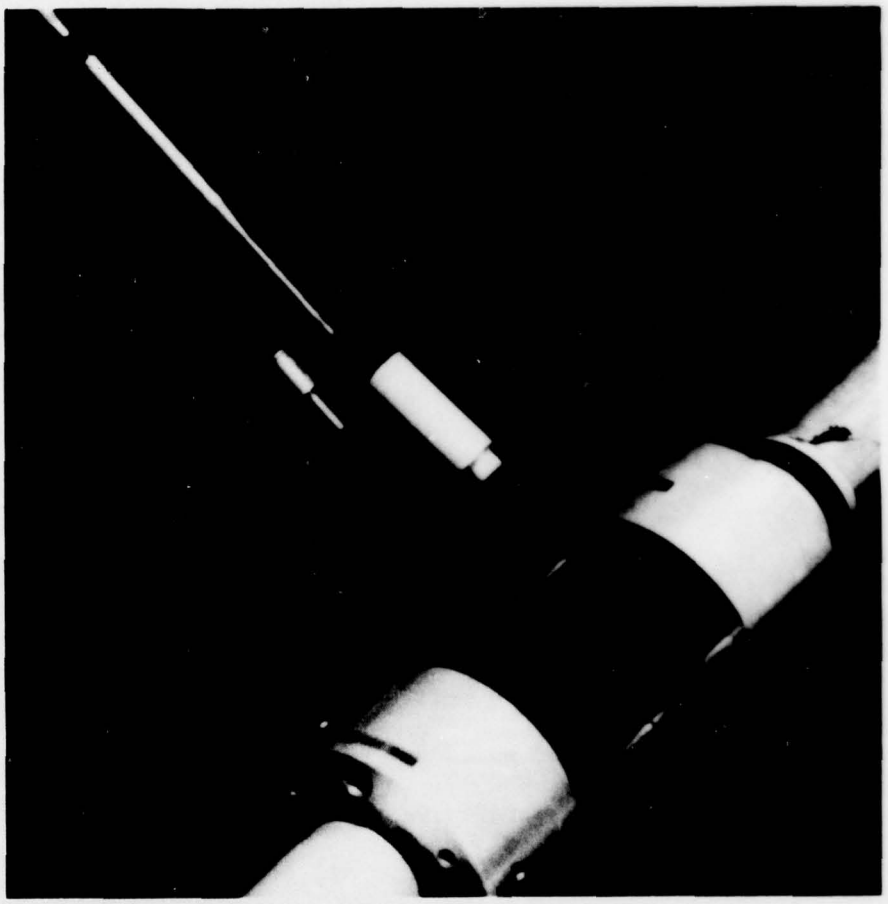

FIGURE 4-3
EXPLODED VIEW OF FLANGE ASSEMBLY WITH MEASURING MICROPHONE AND PLUG

(THE PROTECTIVE GRID SHOWN ON THE MICROPHONE WAS REMOVED BEFORE THE MICROPHONE WAS INSERTED IN THE HOLDER AND FLANGE)

Taken from Ref. 15

to mount flush with the inside surface of the tube wall. When the microphone was not used, an aluminum plug (shown directly below the microphone in Fig. 4-3) was installed. The termination was designed by Williams,[8] on the basis of a paper by Burns.[25] The first part of the termination was a tapered section about 1 m long. The second part, also 1 m long, completely filled the pipe cross section. The reflection coefficients of the termination were measured by a pulse method; the results are given in Chapter 5.

3. The Receiving System

The following pieces of equipment were used in the receiving system.

(1) Microphone. B&K type 4136, 1/4 in. The pressure response of this microphone is flat to within ±0.5 dB from 50 Hz to 70 kHz. When flush mounted in the tube wall, however, the microphone acts as a baffled circular piston receiver. Because the sound waves are incident at 90° to the piston, the 3 dB down frequency response of the microphone is limited to 30 Hz to 28 kHz. All other components in the receiving system have a 3 dB down response of at least 20 Hz to 200 kHz. The microphone is therefore the limiting element in the receiving system.

(2) Preamplifier. B&K type 2619.

(3) Preamplifier and Power Supply. B&K type 2803 dual channel.

(4) Microphone Cables. B&K type AD0029 30 m cables.

(5) Microphone Calibrator (not shown in Fig. 4-1). B&K type 4220 pistonphone. The output of the calibrator is a 240 Hz

sinusoid with a SPL of 123.8 ±0.2 dB.

(6) Spectrum Analyzer. H-P model 3580A.

(7) Oscilloscope Camera (not shown in Fig. 4-1). H-P model 197-A.

(8) Voltmeter. H-P model 400EL.

(9) Oscilloscope. Tektronix model 545B.

(10) Oscilloscope Camera (not shown in Fig. 4-1). Tektronix model 125.

(11) Preamplifier. This preamplifier was constructed for use as a wideband amplifier with negligible phase distortion. The 3 dB down frequency response of this amplifier is 7 Hz to 700 kHz. There is negligible phase distortion above 100 Hz. The gain of the amplifier is 20 ±0.1 dB from 500 Hz to 200 kHz.

C. Experimental Procedures

Three experiments were conducted in this investigation. The procedures are discussed below.

1. Measurement of Small-Signal Attenuation Coefficients

The procedure here was to generate a low level (SPL = 115 to 120 dB) sinusoid at the source and observe the decay of the signal with distance. The attenuation coefficient at a particular frequency was then obtained from a least squares fit of the plot of measured loss versus distance.

2. Measurement of Pipe Termination Reflectivity

The pulse method was used to measure the reflectivity of the pipe termination. The receiving microphone was placed approximately 1.7 m from the beginning of the pipe termination. The direct (p_d) and reflected (p_r) pulse amplitudes were observed on the oscilloscope and their respective values recorded; the amplitude of the reflected pulse was corrected for the round trip loss caused by tube wall attenuation. The reflection coefficient $\bar{R}$ was determined from the expression

$$\bar{R} = 20 \log_{10} \left[\frac{p_r e^{2\alpha_1 x}}{p_d} \right] . \qquad (4\text{-}1)$$

3. Measurements of Received Acoustic Signal versus Propagation Distance and Source Level

With the available apparatus we could, in principle, vary p_{10}, ω, and x. The most convenient way of testing the various theoretical predictions of saturation was to fix x and ω and vary p_{10}. In this way a family of amplitude response curves was obtained. For the purpose of investigating certain other effects, such as dispersion, it was preferable to hold p_{10} and ω fixed and to vary x. In any case the procedure was to measure the received signal as a function of x or p_{10}. Each measurement consisted of recording an oscillogram and spectrum of the received signal.

4. Measurement Accuracy

The accuracy associated with the measurement of SPL, f, and x was estimated from the various uncertainties in the response of the transmitting and receiving system. The SPL measurements are believed accurate

to ±0.5 dB. The frequency stability of the B&K oscillator was observed to be ±0.2%. Distance measurements are accurate to ±1%.

CHAPTER 5

EXPERIMENTAL AND THEORETICAL RESULTS

A. Introduction

In this chapter the experimental results obtained are given and compared with the theoretical predictions found in Chapter 3. These results are divided into two sections, the first dealing with the salient acoustical properties of the pipe, the second with the high intensity experiment. All computations were made for the measured temperature, relative humidity, and ambient pressure of 20°C, 50%, and 760 mm Hg., respectively.

Some of the data given here have been previously reported. Figures 5-5, 5-8, and 5-10 were reported in Ref. 26. Figure 5-3 was reported in Ref. 27.

B. Acoustical Properties of the Pipe

1. Measurement of Attenuation Coefficients

Figure 5-1 shows the measured frequency dependence of the attenuation coefficient for the pipe. The points are the experimental data and the dashed line is a least squares fit to the data. The solid line is the attenuation given by the Kirchhoff formula (Eq. 2-6). The offset of the two lines is about 10%. This is similar to the findings of Pernet and Payne,[9] (8%), and Pestorius,[8] (10%).

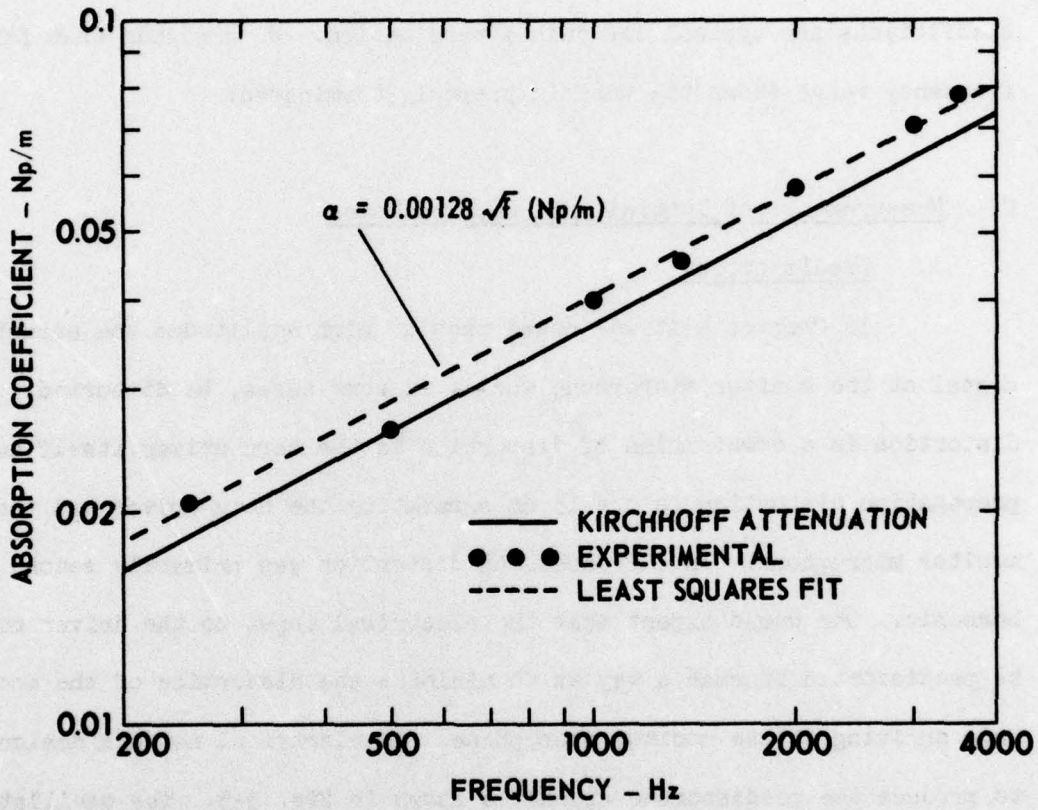

FIGURE 5-1
COMPARISON OF MEASURED ABSORPTION COEFFICIENTS WITH KIRCHHOFF THEORY

2. Measurements of the Termination Reflectivity

As was mentioned in Chapter 4, the reflection coefficients of the termination were measured by the pulse method. A plot of $\bar{R}$, determined from Eq. 4-1, versus frequency is shown in Fig. 5-2. The reflection coefficients are typical for such a termination. We conclude that for the frequency range shown the tube is properly terminated.

C. Measurements of Initially Sinusoidal Waves

1. Predistortion

In Chapter 4 it was noted that at high amplitudes the acoustic signal at the monitor microphone would, in some cases, be distorted. This distortion is a combination of distortion in the horn driver itself and propagation distortion in the 13 cm separating the horn driver and the monitor microphone. In all cases the distortion was primarily second harmonic. One would expect that the electrical input to the driver could be predistorted in such a way as to minimize the distortion of the acoustic wave arriving at the monitor microphone. An electrical network designed to produce the predistorted signal is shown in Fig. 5-3. The oscillator produces a sine wave at the second harmonic of the desired operating frequency. This signal is fed into one input of a summing amplifier and also into a divide-by-two counter. The counter drives the phase-locked oscillator. The phase-locked oscillator produces a sine wave at the operating frequency and serves as the second input to the summing amplifier. The output of the summing amplifier is then the sum of signals at the fundamental and second harmonic frequencies. The phase of the second harmonic

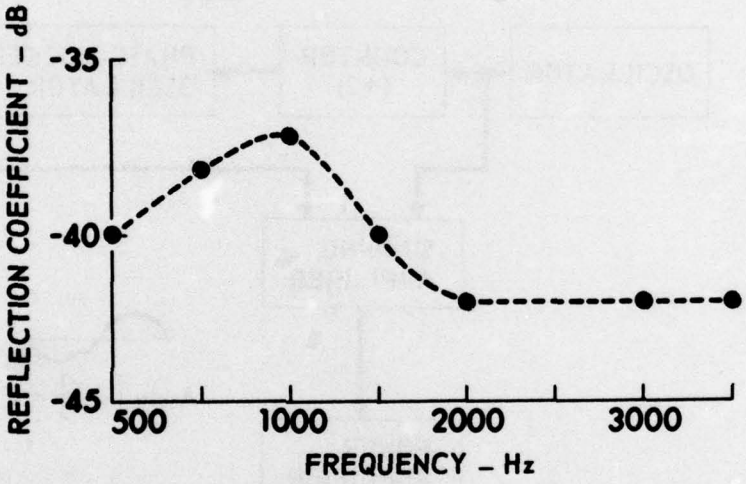

FIGURE 5-2
MEASURED REFLECTION COEFFICIENTS
FOR THE PIPE TERMINATION

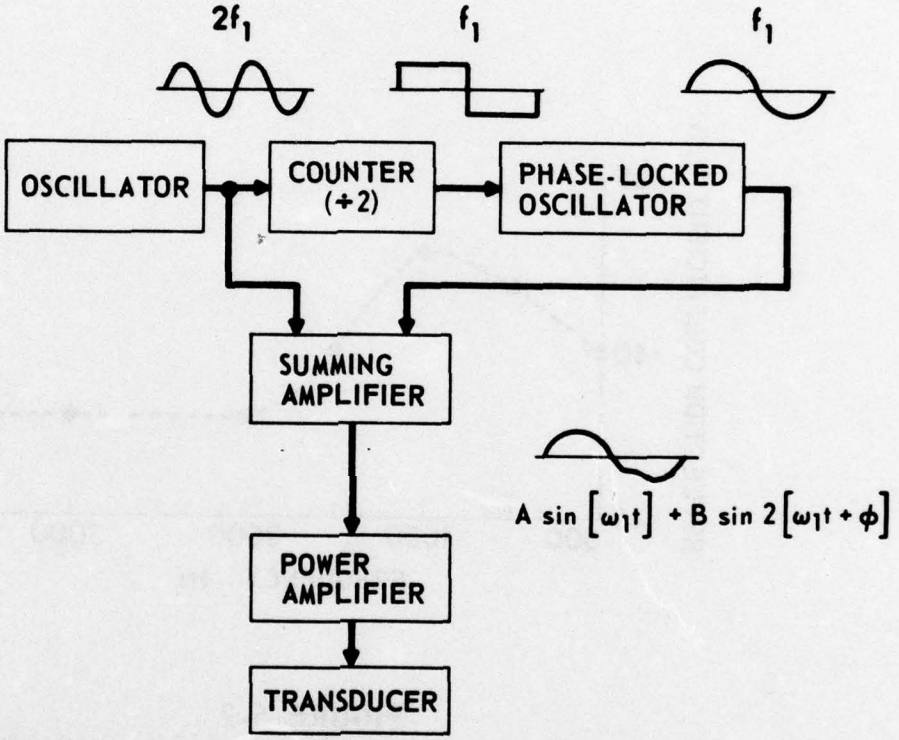

FIGURE 5-3
BLOCK DIAGRAM OF PREDISTORTION NETWORK

component may be varied ±180° with respect to the fundamental by means of a phase control on the phase-locked oscillator.

Typical results using the predistortion network are shown in Fig. 5-4. It is evident that although the electrical input to the driver is a sinusoid the acoustic signal is distorted. Spectral analysis of the acoustic signal shows the presence of a strong second harmonic component 15 dB below the fundamental. The second column of Fig. 5-4 shows the results of using predistortion. When the phase and amplitude of the second harmonic fed to the driver are varied until the second harmonic is minimized at the monitor microphone, a reduction of 22.5 dB in the acoustic second harmonic is achieved.

The main limitation of using predistortion is the bandwidth of the electroacoustic transducer. In our case bandwidth is no limitation because the upper 3 dB down frequency of the driver is 8.5 kHz and our highest fundamental frequency is 4 kHz. With suitable counters the method could be used to suppress any harmonic within the transducer bandwidth.

2. Amplitude Response Curves

The phenomenon of acoustic saturation can most easily be seen from an amplitude response curve taken at a fixed distance. Two such curves are shown in Fig. 5-5. The received SPL at the fundamental frequency is plotted versus source level for two propagation distances at several source frequencies. The dashed lines are predictions based on linear theory, and the solid curves (valid for $\sigma>3$) are the predictions based on the Rudnick model (Eq. 3-12). Saturation is well evidenced by the bending over of the response curves at high source levels. For example, when $f = 3.57$ kHz and $x = 25.8$ m, the extra attenuation is about

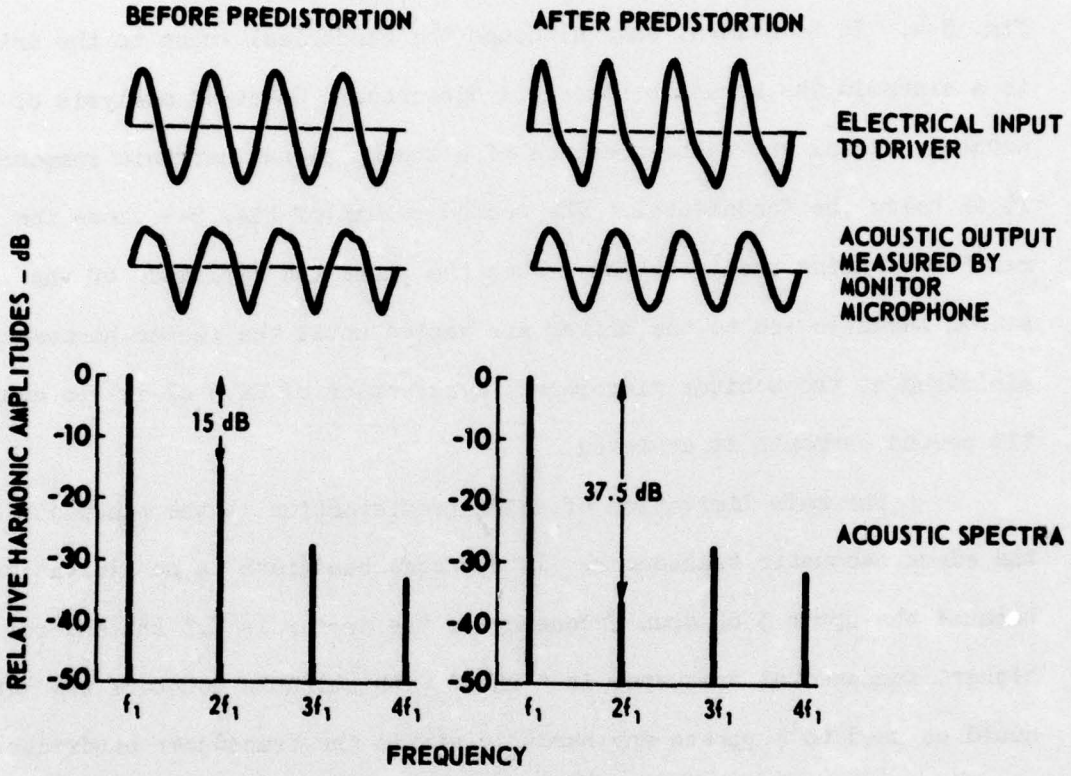

FIGURE 5-4
TYPICAL RESULTS OBTAINED USING THE PREDISTORTION NETWORK (f_1 = 4 kHz)

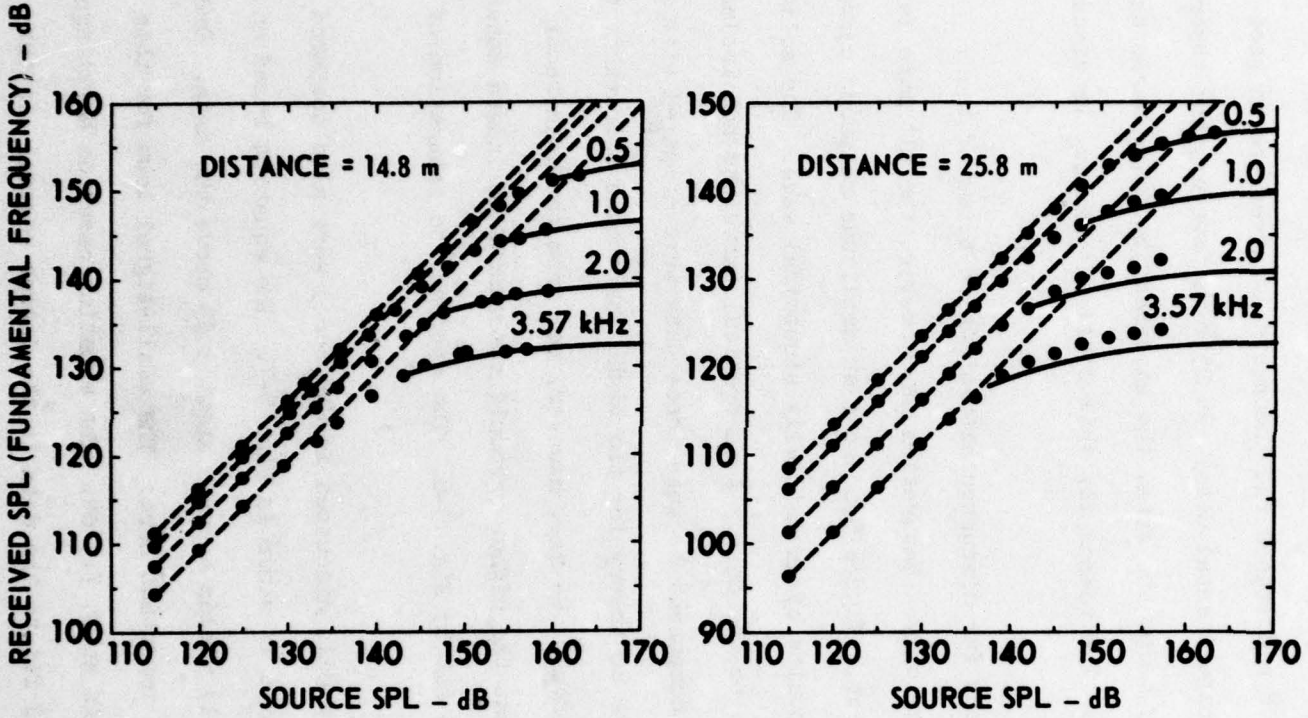

FIGURE 5-5
AMPLITUDE RESPONSE CURVES AT
FUNDAMENTAL FREQUENCY

14.1 dB. At this point 96% of the power at the fundamental frequency has been lost because of nonlinear effects!

At the 14.8 m distance the theoretical curves are in good agreement with the experimental data. At 25.8 m, however, the theoretical curves fall slightly below the data, the agreement becoming worse as the frequency increases. The reason for this small discrepancy is discussed in Chapter 6.

We have thus far discussed saturation in terms of the fundamental frequency only. Saturation is, however, the ultimate fate of each Fourier component. Figure 5-6 shows an amplitude response curve for the first three harmonics of an initially sinusoidal wave. The solid curves are best fits to the data. A theoretical curve was not included for the fundamental component because these data were compared with theory in Fig. 5-5. We have no theory for the higher harmonics comparable to that for the fundamental. We may, however, see from the weak-shock formula (Eq. 2-5) that the higher harmonic components do indeed saturate. This result is borne out by Fig. 5-6. The approach to saturation of each harmonic is evident.

The other models discussed in Chapter 3 were also compared to data. A typical result is shown in Fig. 5-7. The equation based on weak-shock theory (Eq. 3-1) yields a curve about 5 dB above the data. Ordinary absorption is indeed important here. The small-signal loss for this frequency and distance is about 7.5 dB. The equation based on Merklinger's model provides a good fit to the data in the linear region. In the plateau region, however, it yields a curve about 1.3 dB above the data. The equation based on the Rudnick model fits the data to within 0.1 dB.

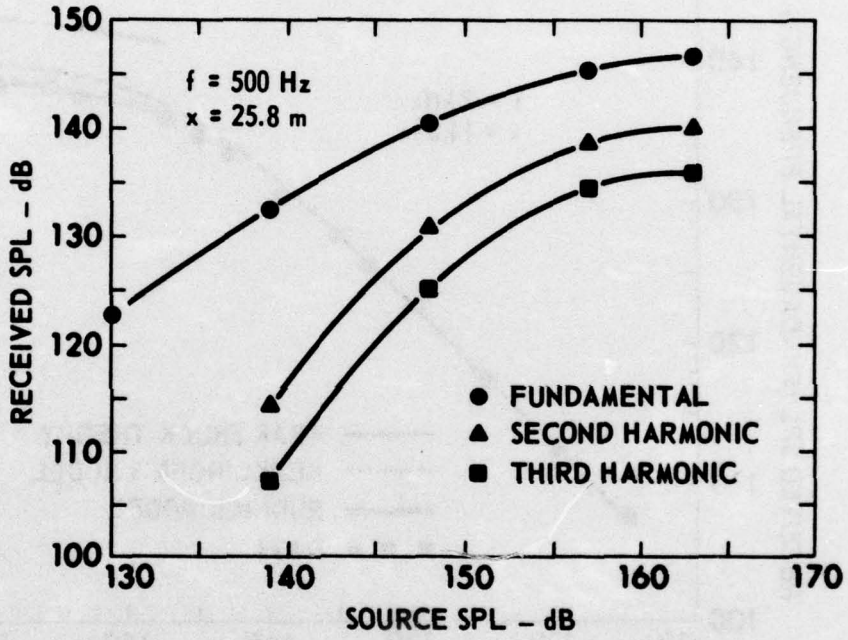

FIGURE 5-6
AMPLITUDE RESPONSE CURVES FOR
THE FIRST THREE HARMONICS OF
AN INITIALLY SINUSOIDAL WAVE

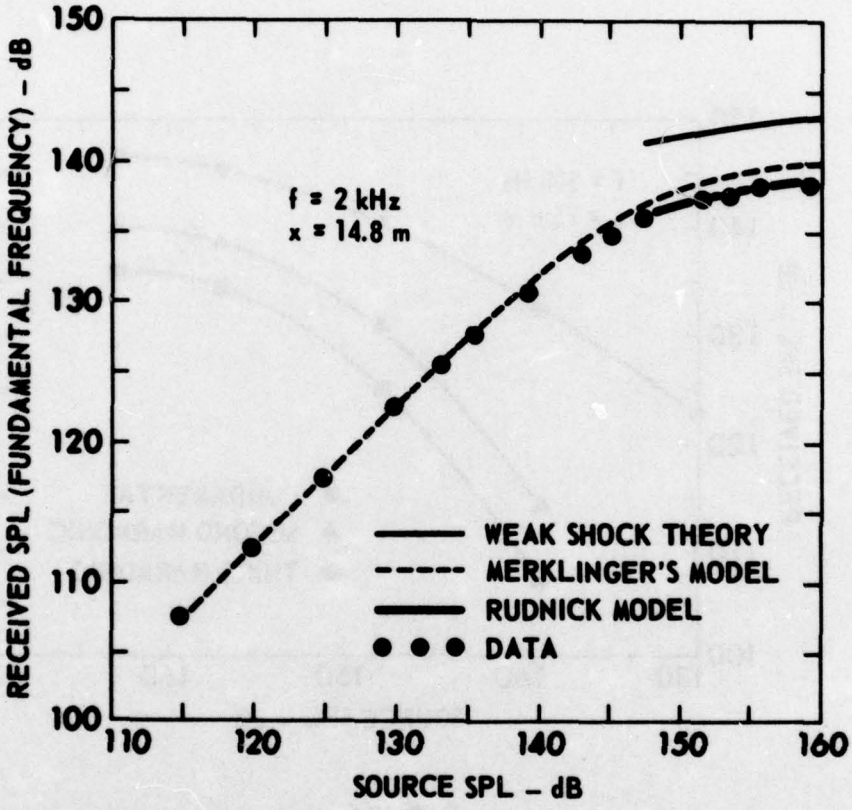

FIGURE 5-7
COMPARISON OF THE VARIOUS THEORETICAL MODELS WITH DATA

In all cases the Rudnick model equation provided a best estimate of the approach to saturation. For this reason the Rudnick model was used as our theoretical model for the rest of this work. The fact that the Rudnick model is limited to waves strong enough to form a sawtooth is not critical for our work because we are interested in saturation and the approach to saturation.

3. Time Waveforms of Received Signals

The received waveforms as a function of source SPL are also of interest. (See Fig. 5-8.) The waveforms at high levels illustrate the strong distortion that is responsible for the extra attenuation. Saturation is evident by inspection of the last two waveforms. The amplitudes are almost the same despite a 5.2 dB difference in the source SPL. It seems likely that the minor "raggedness" in the lower three curves is due to scattering from small irregularities in the pipe near the microphone. These irregularities, probably associated with the flange junction and/or the microphone mounting hole, would be expected to scatter only very high frequencies. Such an expectation is consistent with the fact that the raggedness appears only in waveforms that contain shocks. Note the asymmetry of the waveforms. It begins to show up at 142 dB and is very apparent at 148 dB. The asymmetry is caused by dispersion. The asymmetry is lessened, however, as the source amplitude is increased. See the last two waveforms. Nonlinear effects have become so strong that "steepening" of the shock tends to overcome the rounding of the shock peak.

Modified weak-shock theory is used in Chapter 6 to investigate the effect of dispersion. It is therefore appropriate here to compare our experimental waveforms with those computed using Pestorius' algorithm.

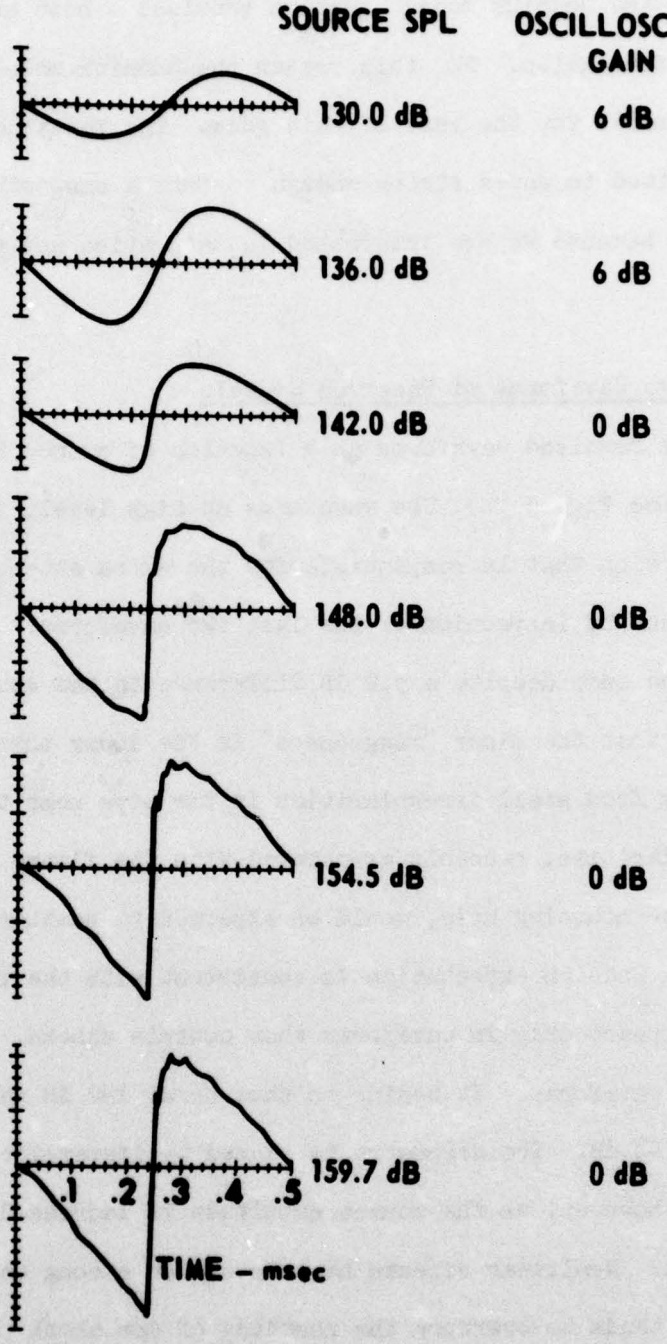

FIGURE 5-8
OSCILLOGRAMS OF RECEIVED SIGNAL FOR VARIOUS SOURCE LEVELS (f = 2 kHz, x = 14.8 m)

Figure 5-9 shows such a comparison. The top waveform in each column is the same because the measured source waveform was used as the source waveform for Pestorius' algorithm. The absorption coefficient used in the computer algorithm is the measured coefficient from Fig. 5-1. We note that the agreement between experiment and theory is quite good in all respects. The progressive distortion of the wave with propagation distance, which is responsible for saturation, is also evident in Fig. 5-9. At 3.7 m the waveform is a sawtooth, though it is slightly asymmetric. As the distance increases the asymmetry grows; the shock peak becomes more rounded while the trough remains sharp. The reason is that as the distance increases the wave amplitude is steadily diminished. Nonlinear effects become too weak to overcome the rounding of the shock peak caused by dispersion.

4. Propagation Curves

Figure 5-10 shows propagation curves for the fundamental component for several different source frequencies. The solid curves are predictions based on the Rudnick model (Eq. 3-11), whereas the dashed curves are those based on weak-shock theory (Eq. 3-1). Each of these curves stops at the left at the distance $x=\hat{x}$ because the predictions are not valid at lesser distances. The dotted line at the top is a small-signal prediction for the 500 Hz case. The point labeled x_{max} is the distance beyond which ordinary absorption is more important than shock dissipation. Beyond x_{max} weak-shock theory is clearly not valid. We note here that for the data shown in Fig. 5-10, the weak-shock formula overestimates the data by about 5 dB at $x=x_{max}$. The Rudnick equation appears to be a great improvement over the weak-shock formula.

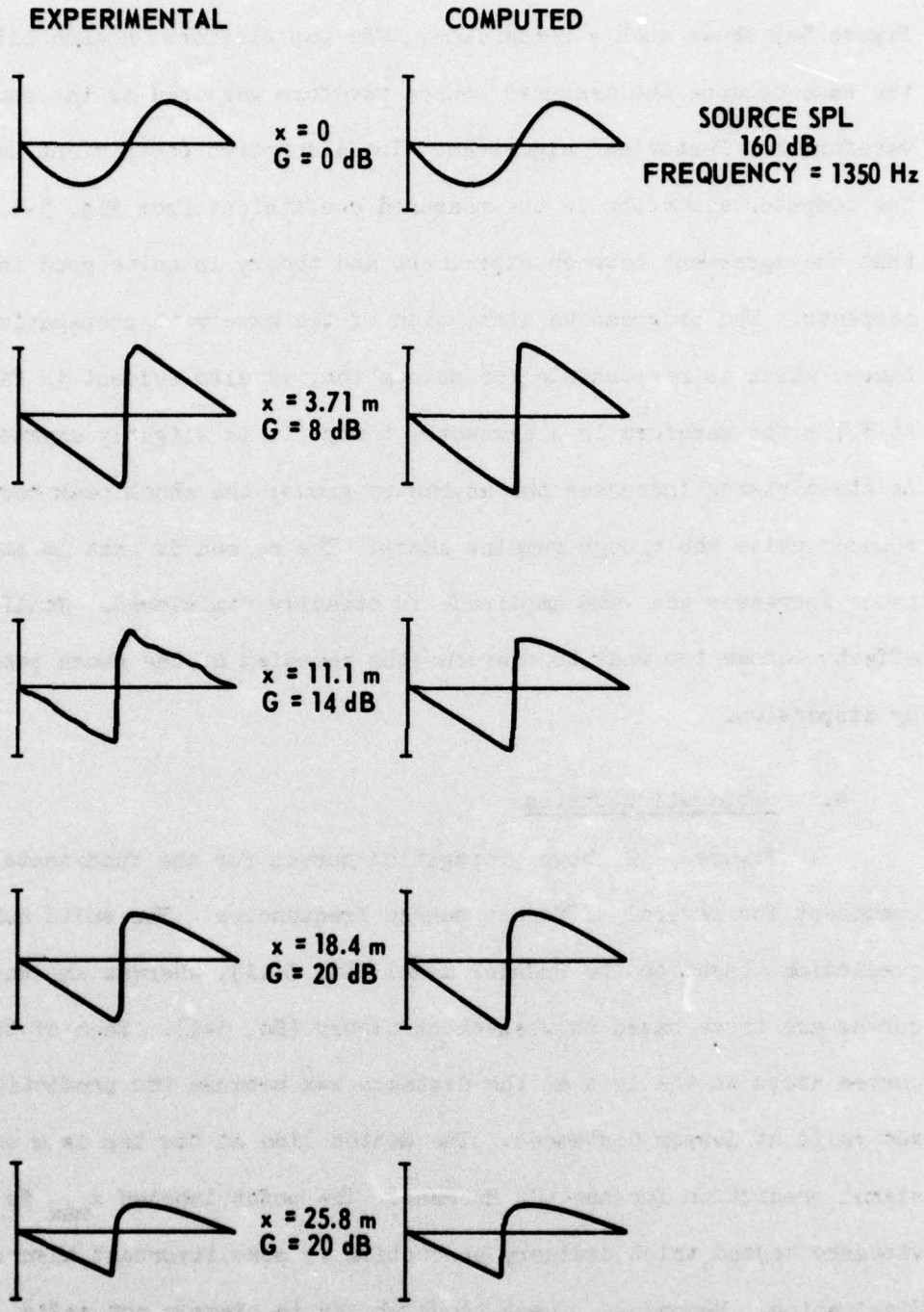

FIGURE 5-9
COMPARISON OF EXPERIMENTAL AND COMPUTED WAVEFORMS AT VARIOUS DISTANCES
(G STANDS FOR OSCILLOSCOPE GAIN)

ARL - UT
AS-76-1338-S
DAW - DR
11 - 11 - 76

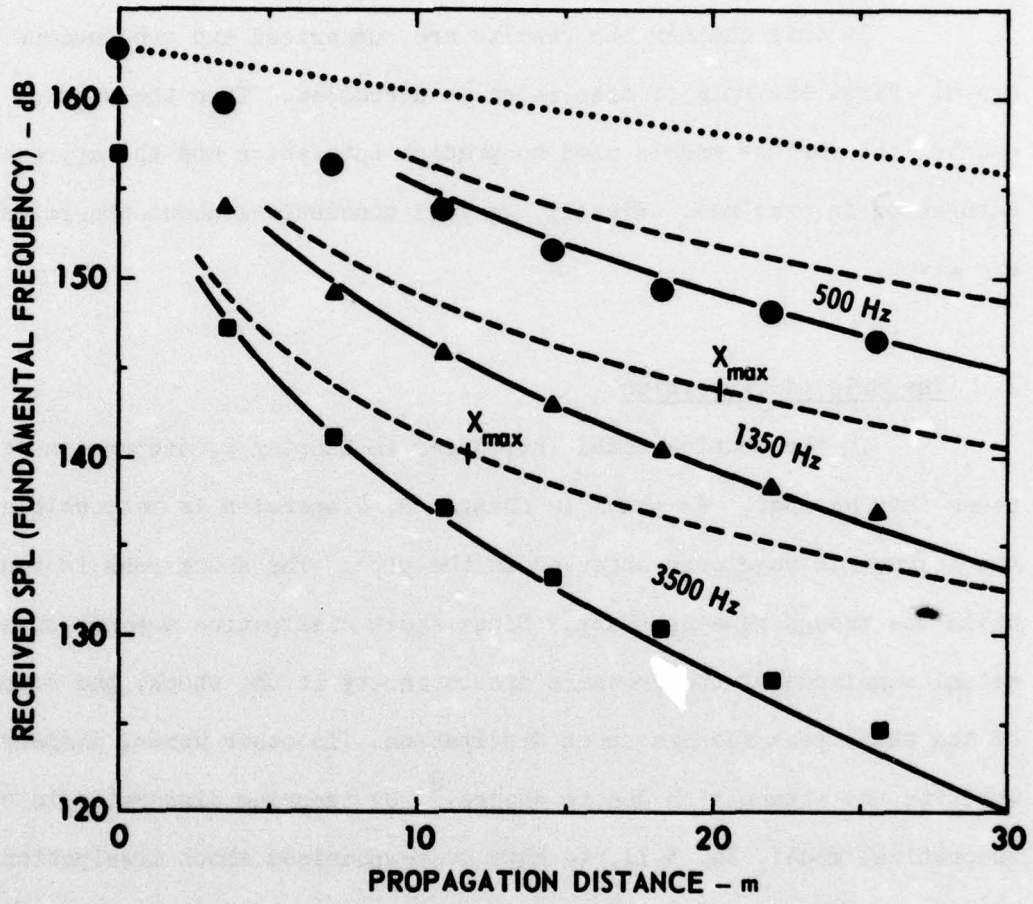

FIGURE 5-10
PROPAGATION CURVES AT VARIOUS FREQUENCIES

CHAPTER 6

CONCLUSIONS

A. Introduction

In this chapter the results are summarized and conclusions are drawn. First the role of dispersion is discussed. Then the success of each of the various models used to predict saturation and the approach to saturation is examined. Finally, general conclusions about the research are given.

B. The Role of Dispersion

In the Rudnick model introduced in Chapter 2, dispersion is not taken into account. As shown in Chapter 2, dispersion is responsible for the asymmetric waveforms observed in the pipe. The shock peak is rounded while the trough remains sharp. Since shock dissipation depends on the actual magnitude of the pressure discontinuity at the shock, the rounding of the shock peak reduces shock dissipation. In other words, dispersion inhibits the attenuation due to shocks.[8] By ignoring dispersion in our theoretical model, Eq. 3-11, we have overemphasized shock dissipation and have therefore arrived at predicted levels that are too low. Furthermore, since the phase shift caused by dispersion depends on the parameter αx, we should expect the discrepancy between prediction and experiment to increase with both frequency and propagation distance. This expectation is qualitatively consistent with the data and curves in Fig. 5-5 and Fig. 5-10.

We have argued here that dispersion could, qualitatively, be responsible for the slight discrepancies observed between data and the Rudnick model at the greater distances and higher frequencies. Pestorius' algorithm was used to find the quantitative effect of dispersion on the received signal. A check on the computer algorithm was made by comparing the predicted propagation curve with experimental data from the tube. (See Fig. 6-1.) The computation was made for the case of a 3.5 kHz plane wave with a source SPL of 157 dB; the experimental value of the absorption coefficient used was $\alpha = 0.078$ Np/m. The agreement with the data is excellent; the maximum deviation is 0.5 dB. To estimate the effect of dispersion on the signal, an additional computer run was made ignoring dispersion effects. The propagation curve obtained from this run is not shown in Fig. 6-1 because it differs at most by 0.1 dB from the curve shown there. We conclude that for this case dispersion has a negligible effect on the amplitude of the fundamental component. Since the given conditions represent the highest frequency and greatest propagation distance in the experiment, dispersion alone cannot account for the small discrepancies between the Rudnick model and the measured data.

The higher harmonic components computed in the two runs are compared in Table 6-1. The harmonic amplitudes with dispersion included (B_n) are compared to those without dispersion (B'_n). The predicted fundamental component of the wave is indeed higher when dispersion effects are included; however, the difference is negligible for the given conditions. Dispersion does, however, seem to become more important for the higher harmonics. This finding is consistent with the observation that the shape of the waveform in the neighborhood of each shock is strongly

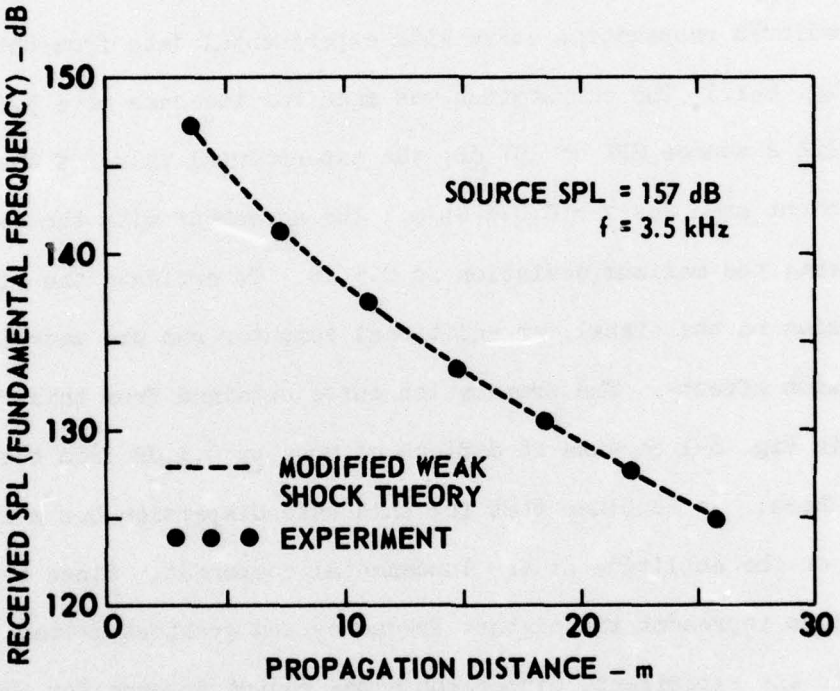

FIGURE 6-1
COMPARISON OF MEASURED PROPAGATION DATA WITH PESTORIUS' ALGORITHM

affected by dispersion. The shock shape is largely determined by the higher harmonic content.

TABLE 6-1

COMPARISON OF COMPUTED HARMONIC AMPLITUDES WITH (B_n) AND WITHOUT (B'_n) DISPERSION CORRECTIONS

Harmonic Number	$20 \log_{10} \left[B_n / B'_n \right]$
1	0.1
2	-0.01
3	-0.2
4	-0.3
5	-0.5
6	-0.6

C. Comparison of The Theoretical Models

1. Modified Weak-Shock Theory

Pestorius' computer algorithm was found to give excellent agreement with the data in all the cases in which it was used. It has two main attractive features. First, it includes the elements of weak-shock theory, small-signal absorption, and dispersion. Second, the source waveform that may be considered is arbitrary. The fact that the algorithm is not an analytic solution made it poorly adapted to our use, however. The computation of an amplitude response curve, for example, would have required a separate computer run for each increment in source level.

2. Modified Merklinger Model

The model suggested by Merklinger to describe the fundamental component of an initially sinusoidal plane wave in a viscous fluid was generalized so that it could be applied to any type of absorbing fluid. The basis of the model is an intensity equation. The primary advantage of this model is that it may be used over the entire range of source level. In all cases near saturation, however, received levels predicted using this model were higher than those actually measured. Typical predicted results are shown in comparison to experimental data in Fig. 5-7.

3. The Rudnick Model

This model was originally used by Rudnick to describe the peak amplitude of a sawtooth wave in the presence of tube wall absorption. The basis of the model is an amplitude equation. We adapted Rudnick's approach to obtain an equation for the decay of the fundamental component p_1. This equation was solved, and predictions were found to be in good agreement with the experimental data. Small discrepancies were found, however. These discrepancies increased with increasing frequency and distance. Dispersion, which was originally thought to be the cause of the small discrepancies, was found to be insignificant for our experimental conditions.

D. Summary and Conclusions

The primary result of this research is the experimental proof of acoustic saturation of plane waves in air. The tendency toward saturation was found to increase with source frequency and/or distance. In one case it was found that nonlinear effects caused 96% of the power at the

fundamental frequency to be lost over a propagation path of 26 m. The transfer of energy to higher frequency components, which is responsible for acoustic saturation, was well evidenced by the formation of sawtooth waves. Dispersion radically alters the time waveform of the received signal (as discussed in Section B of this chapter). However, calculations based on modified weak shock theory show that for our experimental conditions dispersion has negligible effect on the amplitude of the fundamental component.

Another important result of this research is the finding that existing theoretical models, adapted to our experimental conditions, gave a good quantitative explanation of saturation and the approach to saturation. Though weak-shock theory generally indicated the development of saturation, it was necessary to take explicit account of ordinary absorption. We adapted the methods of Rudnick and Merklinger to obtain expressions for the fundamental component p_1. In all cases the Rudnick equation was in better agreement with data.

Some experimental and theoretical results for spherical waves are presented in the appendices.

APPENDICES

In some cases it was possible to generalize the theoretical work done for plane waves to the case of spherically spreading waves. These results are included here as appendices. In Chapter 3, for example, the question of whether ordinary dissipation can prevent the formation of shocks or of a fully formed sawtooth was answered by comparing the critical distances $\bar{x}$, $\hat{x}$, and x_{max}.[3] In Appendix A we discuss a method for assessing the importance of nonlinear effects on spherical waves based on a comparison of the critical ranges $\bar{r}$, $\hat{r}$, and r_{max}. This method leads to a classification of nonlinear effects on spherical waves as weak, moderate, or strong. A perturbation solution of Burgers' equation for weak spherical waves is presented in Appendix B. An extension of the Rudnick model to spherical waves is presented in Appendix C. The model is appropriate for strong waves.

The weak and strong-wave solutions were compared with data from freefield propagation experiments. In both the weak and strong wave experiments the measured quantities were p_1 and p_2 versus range. In the weak-wave experiment the source was an acoustic array; for the strong-wave experiments an acoustic siren was used.

We note here that the material presented in Appendix A was included in Ref. 27.

APPENDIX A

ESTIMATES OF THE IMPORTANCE OF NONLINEARITY ON THE PROPAGATION OF SPHERICAL WAVES

Here we outline a method for estimating the importance of nonlinear effects on the propagation of spherically spreading sound waves. The analysis is based on a comparison of the three critical range parameters $\bar{r}$, $\hat{r}$, and r_{max} corresponding, respectively, to shock formation, sawtooth formation, and "old age." The analysis we present here is somewhat similar to that of Shooter, Muir, and Blackstock.[3] The difference between our approach and that of Shooter et al. is the particular graphical representation of the resulting equations.

The question of when shock or sawtooth formation is possible for a plane wave was dealt with in Chapter 3. The analysis for spherical waves is precisely the same if we replace $\bar{x}$, $\hat{x}$, and x_{max} with $\bar{r}$, $\hat{r}$, and r_{max}, respectively. To find specific formulas for $\bar{r}$, $\hat{r}$, and r_{max}, we first consider the case of an omnidirectional spherical wave. That is, we let the boundary condition be

$$p = p_{10} \sin \omega t \quad , \quad \text{at } r = r_o \quad . \tag{A-1}$$

We assume here that $kr_o \gg 1$. The critical ranges are[3]

$$\bar{r} = r_o e^{1/\beta\epsilon kr_o} , \tag{A-2}$$

$$\hat{r} = r_o e^{3/\beta\epsilon kr_o} , \tag{A-3}$$

$$r_{max} = \frac{\frac{\beta\epsilon kr_o}{\alpha}}{1 + \beta\epsilon kr_o \ln\left(\frac{r_{max}}{r_o}\right)} . \tag{A-4}$$

To simplify the assessment of the importance of nonlinearity, we now consider a graphical display of Eqs. A-2 through A-4. A direct approach would be to plot the three critical distances themselves. If Eqs. A-2 and A-3 are divided by r_o, the normalized quantities $\bar{r}/r_o$ and $\hat{r}/r_o$ may be plotted versus the single parameter $\beta\epsilon kr_o$. The equation for r_{max}/r_o, however, depends on two parameters, $\beta\epsilon kr_o$ and αr_o. A family of curves would therefore have to be plotted to represent r_{max}/r_o. An alternative approach is as follows: a reference point roughly marking the threshold of importance of nonlinearity is $\bar{r}=r_{max}$; far more serious nonlinear effects are indicated by $\hat{r}=r_{max}$. These two equalities define the following relations, respectively:

$$\bar{r} = r_{max} \rightarrow 2\alpha r_o = \beta\epsilon kr_o e^{-1/\beta\epsilon kr_o} , \tag{A-5}$$

and

$$\hat{r} = r_{max} \rightarrow 4\alpha r_o = \beta\epsilon kr_o e^{-3/\beta\epsilon kr_o} . \tag{A-6}$$

Only two dimensionless groups appear in Eqs. A-5 and A-6, $\beta\epsilon kr_o$ and αr_o. This suggests representing these two equations by plotting, for example,

$\beta\epsilon kr_o$ versus αr_o. It is easily seen that for a given medium the quantity $\beta\epsilon kr_o$ depends only on the source level SL (farfield SPL extrapolated to 1 m) and f. A convenient measure of $\beta\epsilon kr_o$ is the "source-frequency level" SFL (dB re 0.0002 μbar-kHz-m) defined as follows:

$$SFL = SL + 20 \log_{10} f_{kHz} \quad , \tag{A-7}$$

where f_{kHz} is the frequency in kilohertz. The SFL as we have defined it here is what Merklinger, Mellen, and Moffet[29] call the "scaled source level" SL*. The relation between SFL and $\beta\epsilon kr_o$ for air at 20°C is

$$SFL = 167.2 + 20 \log_{10} \beta\epsilon kr_o \quad . \tag{A-8}$$

Figure A-1 shows plots of Eqs. A-5 and A-6 in terms of SFL and αr_o.

Figure A-1 may be used in the following way to assess the general importance of nonlinear effects on the propagation of spherical waves in air. Nonlinear effects are expected to be weak, moderate, or strong if the value of SFL and αr_o defines a point below, between, or above the two curves, respectively. The reason is this: points below the two curves define waves for which $r_{max} < \bar{r}$, i.e., shocks never form; points between the two curves depict waves for which $\bar{r} < r_{max} < \hat{r}$, i.e., shocks form but a sawtooth does not; points above the two curves define waves for which $\hat{r} < r_{max}$, i.e., both shock and sawtooth formation is possible. The points B and C in Fig. A-1 represent the operating points for the experiments presented in Appendices B and C, respectively, and are discussed there.

We emphasize here that Fig. A-1 contains no information regarding the length scale for the development of the nonlinear effects. That is, one may, for example, find that for a given set of source parameters the corresponding values of SFL and αr_o define a point well

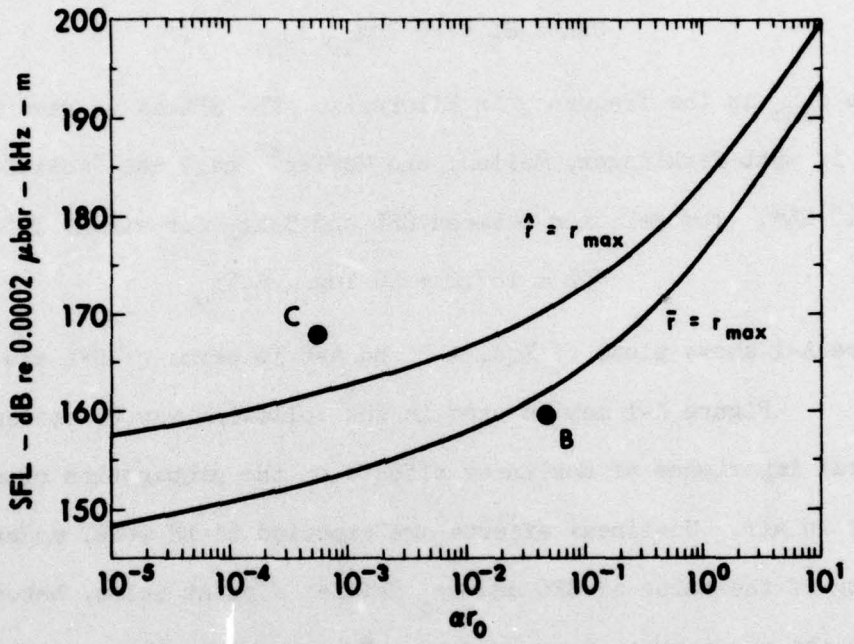

FIGURE A-1
DESIGN CURVE TO ASSESS THE IMPORTANCE OF NONLINEARITY ON SPHERICAL WAVE PROPAGATION
(CONDITIONS ARE FOR AIR AT 20°C)

above the $\hat{r}=r_{max}$ curve. Calculation of the distances $\bar{r}$ and $\hat{r}$ may, however, show that $\bar{r}$ falls well beyond the distance at which experimental observations will be made. Hence, nonlinear effects would be of little importance for the given length scale. In summary, if use of Fig. A-1 shows that nonlinear effects may be important, then computation of the range parameters themselves must be made to set the length scale of the development of the effects.

In most practical cases the acoustic source is not a vibrating sphere but a directional radiator, such as a baffled piston or an acoustic horn. Though we have considered an omnidirectional source, our results may be extended to directional waves by replacing p_{10} in Eq. A-1 with $p_{10}D(\theta)$, where $D(\theta)$ is the normalized directivity function.[30] But the value of r_o, the effective source radius, needs to be specified. If there is no distortion in the nearfield of the radiator, it is appropriate to take $r_o=R_o$, where R_o is the length of the nearfield. Unfortunately, however, this is seldom the case. Nonlinear effects cause the signal to distort as it propagates through the nearfield. Several researchers have investigated this problem empirically and found that choosing r_o in the range $R_o/3<r_o<3R_o/4$ works fairly well for piston-type radiators.[3] Apparently choosing r_o in this range gives about the right weight to the distortion that takes place in the nearfield.

At this point, we include experimental data to illustrate the validity of using the three critical distances to assess the importance of nonlinear effects. Unfortunately, the data we have is for plane waves, not spherical waves. However, the basic concept is the same, no matter what the geometry of the wave motion may be. Figure A-2 shows waveforms

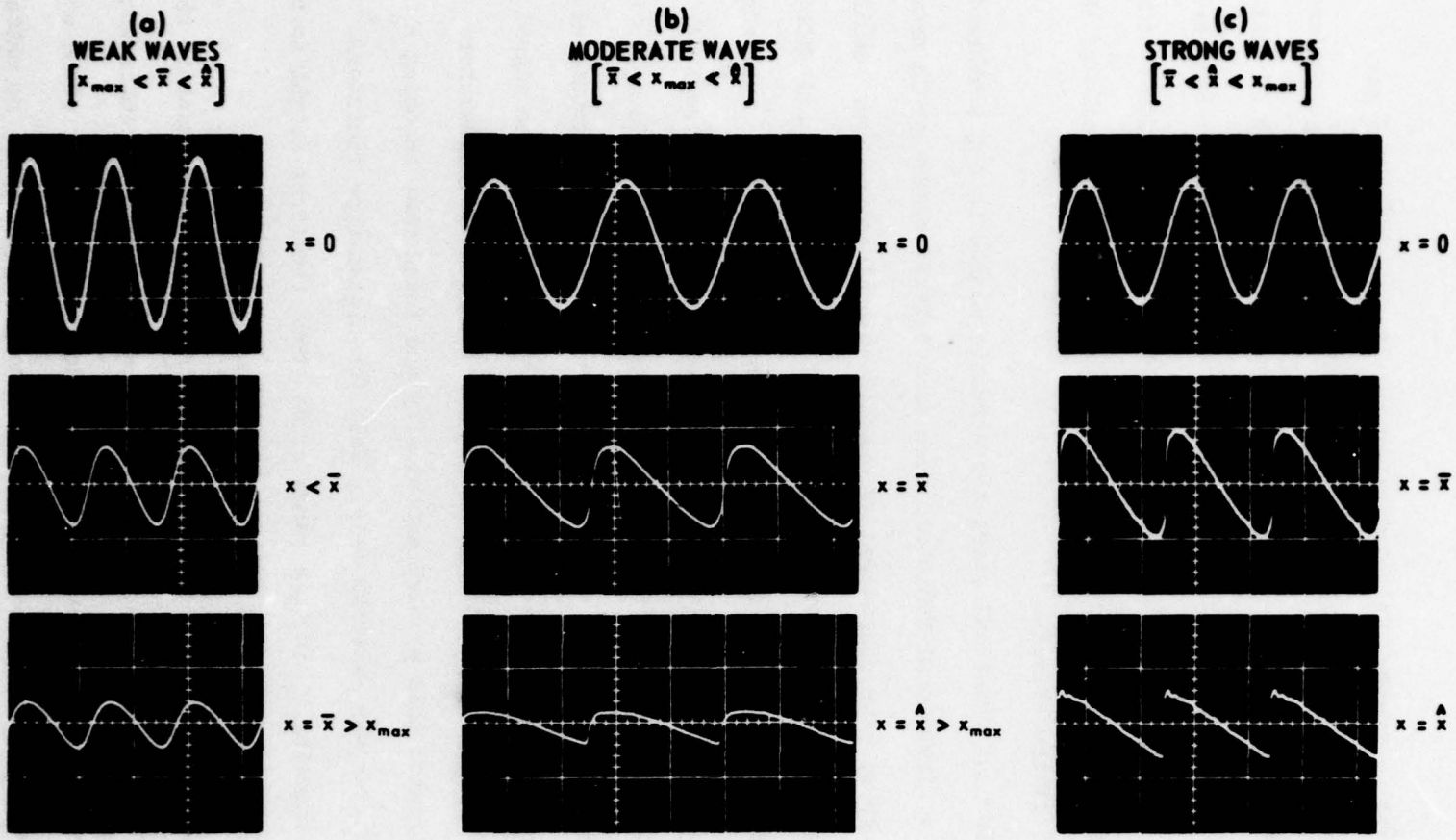

FIGURE A-2
MEASURED WAVEFORMS CORRESPONDING TO WEAK, MODERATE, AND STRONG NONLINEARITY

for the case of weak, moderate, and strong nonlinearity. The condition $x_{max}<\bar{x}$ holds for the first set of wavesforms, Fig. A-2(a). Under this condition, shocks are not expected. Notice, indeed, that a shock never forms. The steepening at $x=\bar{x}$ is less than that measured at the second distance. The reason is that the high frequency components damp out before a shock can form. Figure A-2(b) shows measured waveforms consistent with the condition $\bar{x}<x_{max}<\hat{x}$. At the second distance ($x=\bar{x}$) considerable steepening is present though the shock is not fully formed. At the third distance ($x=\hat{x}$) the wave is slightly more distorted than at the second distance, but certainly it is not a full fledged sawtooth. The peculiar wave shape at $x=\hat{x}$ is caused by dispersion and is discussed in detail in Chapter 2. Figure A-2(c) depicts the case $\hat{x}<x_{max}$. At the distance $x=\bar{x}$ shock formation is very apparent, and the characteristic sawtooth shape is evident at $x=\hat{x}$. We conclude that the critical distance method is in good qualitative agreement with the data of Fig. A-2.*

In summary Fig. A-1, used in conjunction with Eqs. A-2 through A-4, should be quite useful in estimating the importance of nonlinearity on the propagation of spherically spreading sound waves. While the approach is not new (see Ref. 3), the particular graphical representation is.

---

*Experimental data for spherical waves is given in Ref. 28.

APPENDIX B

A PERTURBATION SOLUTION OF BURGERS' EQUATION FOR SPHERICAL WAVES

Our purpose here is to obtain a theoretical prediction valid for weak spherical waves in a thermoviscous fluid. Several other researchers have obtained results valid for the weak-wave problem.[9,31-33] Pernet and Payne,[9] for example, extended the phenomenological approach of Thuras et al.[23] to the spherical wave problem. Blackstock and Willette,[33] however, obtained a perturbation solution of Burgers' equation valid to third order in the source Mach number ϵ. The work we present here is an extension of Blackstock's et al. perturbation analysis to fifth order in ϵ. We also show a limited test of the theoretical results by comparison with data from an outdoor propagation experiment.

The Burgers' equation for spherical waves is (see, for example, Ref. 1)

$$\frac{1}{r}\frac{\partial(ru)}{\partial r} - \frac{\alpha}{\omega^2}\frac{\partial^2 u}{\partial t'^2} = \frac{\beta}{c_o^2}\, u\, \frac{\partial u}{\partial t'} \quad , \tag{B-1}$$

where α is the thermoviscous absorption coefficient at angular frequency ω and $t'=t-(r-r_o/c_o)$ is the retarded time. Let the boundary condition be

$$u(r_o,t) = u_{10} \sin \omega t \quad . \tag{B-2}$$

It is convenient here to cast Eqs. B-1 and B-2 in terms of the dimensionless quantities $V=(r/r_o)(u/c_o)$ and $y=\omega t'$. Making the substitutions for V and y and also defining $\zeta=\beta k r_o$, Eqs. B-1 and B-2 become

$$\frac{\partial V}{\partial r} - \alpha \frac{\partial^2 V}{\partial y^2} = \frac{\zeta}{r} V \frac{\partial V}{\partial y} \quad , \tag{B-3}$$

and

$$V(r_o, y) = \epsilon \sin y \quad , \tag{B-4}$$

respectively. We seek a solution of Eq. B-3 in the form of a perturbation series. That is, we suppose a solution of the form

$$V = \sum_{n=1}^{\infty} \epsilon^n V^{(n)} \quad . \tag{B-5}$$

Substituting Eq. B-5 into Eq. B-3, we obtain

$$\sum_{n=1}^{\infty} \epsilon^n \left[\frac{\partial V^{(n)}}{\partial r} - \alpha \frac{\partial^2 V^{(n)}}{\partial y^2} - \frac{\zeta}{r} \sum_{i+j=n} V^{(i)} \frac{\partial V^{(j)}}{\partial y} \right] = 0 \quad . \tag{B-6}$$

In order that Eq. B-6 be satisfied, the bracketed term must vanish for each value of n. In general the resulting differential equations corresponding to terms of order ϵ^n (denoted $O(\epsilon^n)$) may be written as

$$O(\epsilon^n) \rightarrow \frac{\partial V^{(n)}}{\partial r} - \alpha \frac{\partial^2 V^{(n)}}{\partial y^2} = \frac{\zeta}{r} \sum_{i+j=n} V^{(i)} \frac{\partial V^{(j)}}{\partial y} \quad . \tag{B-7}$$

We see that in general the equations must be solved in sequence. For example, the source terms for the second order solution $V^{(2)}$ depend on $V^{(1)}$. The source terms for the third order solution $V^{(3)}$ depend on $V^{(2)}$ and $V^{(1)}$. We now proceed to solve the first five such equations.

The first order equation is

$$\frac{\partial V^{(1)}}{\partial r} - \alpha \frac{\partial^2 V^{(1)}}{\partial y^2} = 0 \quad . \tag{B-8}$$

Hence, the first order solution $V^{(1)}$, which satisfies the boundary condition Eq. B-4, is

$$V^{(1)} = e^{-\alpha(r-r_o)} \sin y \quad , \tag{B-8a}$$

which is the familiar solution of linear acoustics. The second order equation is

$$\frac{\partial V^{(2)}}{\partial r} - \alpha \frac{\partial^2 V^{(2)}}{\partial y^2} = \frac{\zeta}{r} V^{(1)} \frac{\partial V^{(1)}}{\partial y} = \frac{\zeta}{2r} e^{-2\alpha(r-r_o)} \sin 2y \quad . \tag{B-9}$$

The solution of Eq. B-9 may be found by assuming $V^{(2)}=F(r) \sin 2y$. The result is

$$V^{(2)} = \frac{\zeta}{2} e^{-4\alpha(r-r_o)} I_{22} \sin 2y \quad , \tag{B-9a}$$

where

$$I_{22} = \int_{r_o}^{r} \frac{e^{2\alpha(r'-r_o)}}{r'} dr' \quad .$$

We shall have occasion to write down several integrals of the form I_{mn} and adopt the following convention. The integral I_{mn} means the integral which must be evaluated to obtain the contribution to the nth harmonic from the mth order perturbation.

The third order solution $V^{(3)}$ satisfies

$$\frac{\partial V^{(3)}}{\partial r} - \alpha \frac{\partial^2 V^{(3)}}{\partial y^2} = \frac{\zeta}{r}\left[\frac{\partial (V_1 V_2)}{\partial y}\right] \quad , \tag{B-10}$$

$$= \frac{\zeta^2}{4r} I_{22}\, e^{-5\alpha(r-r_o)} [3 \sin 3y - \sin y] \quad .$$

The solution of Eq. B-10 may be found by assuming $V^{(2)}=G(r)\sin y+F(r)\sin 3y$. The result may be written as

$$V^{(3)} = -\frac{\zeta^2}{4} I_{31}\, e^{-\alpha(r-r_o)} \sin y + \frac{3\zeta^2}{4} I_{33}\, e^{-9\alpha(r-r_o)} \sin 3y \quad , \tag{B-10a}$$

where

$$I_{31} = \int_{r_o}^{r} \frac{I_{22}(r')\, e^{-4\alpha(r'-r_o)}}{r'}\, dr' \quad ,$$

and

$$I_{33} = \int_{r_o}^{r} \frac{I_{22}(r')\, e^{4\alpha(r'-r_o)}}{r'}\, dr' \quad .$$

We see that the third order solution gives rise to a term which describes the initial decay of the fundamental and the initial growth of the third harmonic.

The fourth order equations and solution are listed below.

$$\frac{\partial V^{(4)}}{\partial r} - \alpha \frac{\partial^2 V^{(4)}}{\partial y^2} = \frac{\zeta}{r}\left[V^{(2)}\frac{\partial V^{(2)}}{\partial y} + \frac{\partial (V^{(1)}V^{(3)})}{\partial y}\right]$$

$$= \frac{\zeta^3}{4r}\left[\left(-I_{31}\, e^{-2\alpha(r-r_o)} - 3I_{33}\, e^{-10\alpha(r-r_o)}\right)\sin 2y\right. \tag{B-11}$$

$$\left. + \left(I_{22}{}^2\, e^{-8\alpha(r-r_o)} + 6I_{33}\, e^{-10\alpha(r-r_o)}\right)\sin 4y\right]$$

$$V^{(4)} = \frac{\zeta^3}{4}\left[-(I_{42}+3I'_{42})\, e^{-4\alpha(r-r_o)}\sin 2y\right. \tag{B-11a}$$

$$\left. + (I_{44}+6I'_{44})\, e^{-16\alpha(r-r_o)}\sin 4y\right]$$

$$I_{42} = \int_{r_o}^{r} \frac{I_{31}(r')\, e^{2\alpha(r'-r_o)}}{r'}\, dr'$$

$$I'_{42} = \int_{r_o}^{r} \frac{I_{33}(r')\, e^{-6\alpha(r'-r_o)}}{r'}\, dr'$$

$$I_{44} = \int_{r_o}^{r} \frac{I_{22}{}^2(r')\, e^{8\alpha(r'-r_o)}}{r'}\, dr'$$

$$I'_{44} = \int_{r_o}^{r} \frac{I_{33}(r')\, e^{6\alpha(r'-r_o)}}{r'}\, dr'$$

Because of the rather formidable algebra involved, the only part of the fifth order solution that was calculated was the contribution to the fundamental. This contribution is denoted $V^{(5)}_{\text{fund.}}$. The results are listed below.

$$\frac{\partial v^{(5)}}{\partial r} - \alpha \frac{\partial^2 v^{(5)}}{\partial y^2} = \frac{\zeta}{r}\left[\frac{\partial\left(v^{(1)}v^{(4)}\right)}{\partial y} + \frac{\partial\left(v^{(2)}v^{(3)}\right)}{\partial y}\right] \tag{B-12}$$

$$v^{(5)}_{\text{fund.}} = \frac{\zeta^4}{8} e^{-\alpha(r-r_o)}\left[I_{51} - \frac{3}{2} I'_{51}\right] \tag{B-12a}$$

$$I_{51} = \int_{r_o}^{r}\left[I_{42}(r') + 3I'_{42}(r') + \frac{I_{22}(r')\, I_{31}(r')}{2}\right]\frac{e^{-4\alpha(r'-r_o)}}{r'}\, dr'$$

$$I'_{51} = \int_{r_o}^{r}\frac{I_{22}(r')\, I_{33}(r')\, e^{-12\alpha(r'-r_o)}}{r'}\, dr' \quad .$$

As may be seen from the higher order results, the solutions are easy to write down in terms of the integrals I_{mn}. It is the calculation of these integrals which is indeed a formidable task.

Let us now put our results in terms of the normalized harmonic amplitudes $B_n=(r/r_o)(u_n/u_o)$. Defining $\sigma_o=\epsilon\zeta$, we obtain

$$B_1 = e^{-\alpha(r-r_o)}\left[1 - \frac{\sigma_o^2}{4} I_{31} + \frac{\sigma_o^4}{8}\left(I_{51} - \frac{3}{2} I'_{51}\right)\right] \quad , \tag{B-13}$$

$$B_2 = e^{-4\alpha(r-r_o)}\left[\frac{\sigma_o}{2} I_{22} - \frac{\sigma_o^3}{4}\left(I_{42}+3I'_{42}\right)\right] \quad , \tag{B-14}$$

$$B_3 = e^{-9\alpha(r-r_o)}\left[\frac{3\sigma_o^2}{4} I_{33}\right] \quad , \tag{B-15}$$

$$B_4 = e^{-16\alpha(r-r_o)} \left[\frac{\sigma_o^3}{4} (I_{44}+6I'_{44}) \right] \quad . \tag{B-16}$$

As a check on our theoretical results, we now inquire as to the behavior of the solutions B_n in the limit of small values of αr. We expect that these limiting forms should correspond to the harmonic amplitudes found from the Bessel-Fubini solution (see, for example, Ref. 12), which are given by

$$B_n = \frac{2}{n\sigma} J_n (n\sigma) \quad , \tag{B-17}$$

where $\sigma=\beta\epsilon kr_o \ln(r/r_o)$. To compare our solution to Eq. B-17, we first establish the limiting forms of the integrals I_{mn}. In the limit as $\alpha r \to 0$, the integrals I_{mn} reduce to the following.

$$I_{22} = \ln \frac{r}{r_o} \tag{B-18a}$$

$$I_{31} = \ln^2 \frac{r}{r_o} \tag{B-18b}$$

$$I_{33} = \frac{1}{2} \ln^2 \frac{r}{r_o} \tag{B-18c}$$

$$I_{42} = \frac{1}{6} \ln^3 \frac{r}{r_o} \tag{B-18d}$$

$$I'_{42} = \frac{1}{6} \ln^3 \frac{r}{r_o} \tag{B-18e}$$

$$I_{44} = \frac{1}{3} \ln^3 \frac{r}{r_o} \tag{B-18f}$$

$$I'_{44} = \frac{1}{6} \ln^3 \frac{r}{r_o} \tag{B-18g}$$

$$I_{51} = \frac{11}{48} \ln^4 \frac{r}{r_o} \tag{B-18h}$$

$$I'_{51} = \frac{1}{8} \ln^4 \frac{r}{r_o} \quad . \tag{B-18i}$$

The expressions for the harmonic amplitudes B_n are, in the limit as $\alpha r \to 0$,

$$B_1 = 1 - \frac{\sigma^2}{8} + \frac{\sigma^4}{192} \quad , \tag{B-19}$$

$$B_2 = \frac{\sigma}{2} - \frac{\sigma^3}{6} \quad , \tag{B-20}$$

$$B_3 = \frac{3\sigma^2}{8} \quad , \tag{B-21}$$

$$B_4 = \frac{\sigma^3}{3} \quad . \tag{B-22}$$

Comparison of Eqs. B-19 through B-22 with the series expansion of Eq. B-17 shows that our results are consistent with the Bessel-Fubini solution to the orders of σ which we have kept. For example, Eq. B-19 is the series expansion of Eq. B-17 to fourth order in σ. Hence, the results of the perturbation solution (Eqs. B-13 through B-16) do indeed reduce to the Bessel-Fubini solution as $\alpha r \to 0$.

In many cases where such a perturbation solution is useful, some distortion is evident in the source waveform $V(r_o, y)$. Commonly this distortion is primarily second harmonic (especially if it is due to nonlinear propagation distortion in the nearfield). We shall now

determine how the presence of an "initial" second harmonic signal changes the lower order perturbation results. Suppose that, in place of Eq. B-4, the boundary condition is

$$V(r_o,y) = \epsilon\left[\sin y + a \sin(2y+\varphi)\right] \quad , \tag{B-23}$$

where a and φ are the relative amplitude and phase of the second harmonic, respectively. The first order perturbation solution satisfying this boundary condition is

$$V^{(1)} = e^{-\alpha(r-r_o)} \sin y + a\, e^{-4\alpha(r-r_o)} \sin(2y+\varphi) \quad . \tag{B-24}$$

The second order solution $V^{(2)}$ has a source term proportional to $V^{(1)}(\partial V^{(1)}/\partial y)$. Hence, it is easily seen that $V^{(2)}$ contains contributions to the first, second, third, and fourth harmonics. The expression for $V^{(2)}$ is

$$V^{(2)} = -\frac{a\zeta}{2} e^{-\alpha(r-r_o)} I_{21} \sin(y+\varphi) + \frac{\zeta}{2} e^{-4\alpha(r-r_o)} I_{22} \sin 2y + F(r) \sin(3y+\varphi) + G(r) \sin(4y+2\varphi) \quad , \tag{B-25}$$

where $I_{21} = \int_{r_o}^{r} \frac{e^{-4\alpha(r'-r_o)}}{r'}\, dr'$.

We note here that the second harmonic component of $V^{(2)}$ is not affected by the "initial" second harmonic. The expressions for B_1 and B_2 are, then, to second order

$$B_1 = e^{-\alpha(r-r_o)} \left(1 + \left(\frac{a\sigma_o}{2}\right)^2 I_{21}^{\,2} - a\sigma_o I_{21} \cos\varphi\right)^{1/2} , \quad \text{(B-26)}$$

and

$$B_2 = e^{-4\alpha(r-r_o)} \left(1 + \frac{\sigma_o^2}{4} I_{22}^{\,2} + \sigma_o I_{22} \cos\varphi\right)^{1/2} . \quad \text{(B-27)}$$

We now wish to compare the results of the perturbation analysis with data from an outdoor propagation experiment. In particular we wish to compare the measured values of p_1 and p_2 with the perturbation analysis for a boundary condition similar to Eq. B-23. The source was an array of seven electroacoustic drivers with exponential horns.[28] A side view of the array is shown in Fig. B-1. The diameter and transmitting frequency of the array were 0.5 m and 8.25 kHz, respectively. The absorption coefficient α was 0.0076 Np/m. The amplitudes p_1 and p_2 at the beginning of the farfield (r_o=6.1 m) were 551 μbar and 143 μbar, respectively, and the phase angle φ was observed to be zero. In terms of the parameters discussed in Appendix A, the operating conditions for this experiment are SFL=159.8 dB, αr_o=0.046. These conditions determine a point on Fig. A-1 (point B) that falls below the $\bar{r}=r_{max}$ curve; therefore the perturbation analysis should be valid. Figure B-2 shows the measured data and theoretical results. Since the wave is weak, the linear theory result (Eq. B-8a) describes the behavior of p_1 fairly well, though the second order perturbation result (dashed curve) provides a slightly better fit at the greater ranges. The lower solid curve is the linear theory prediction for p_2. The dotted curve is the second order perturbation result for p_2 for no initial second harmonic (Eq. B-9a). Since the phase difference φ

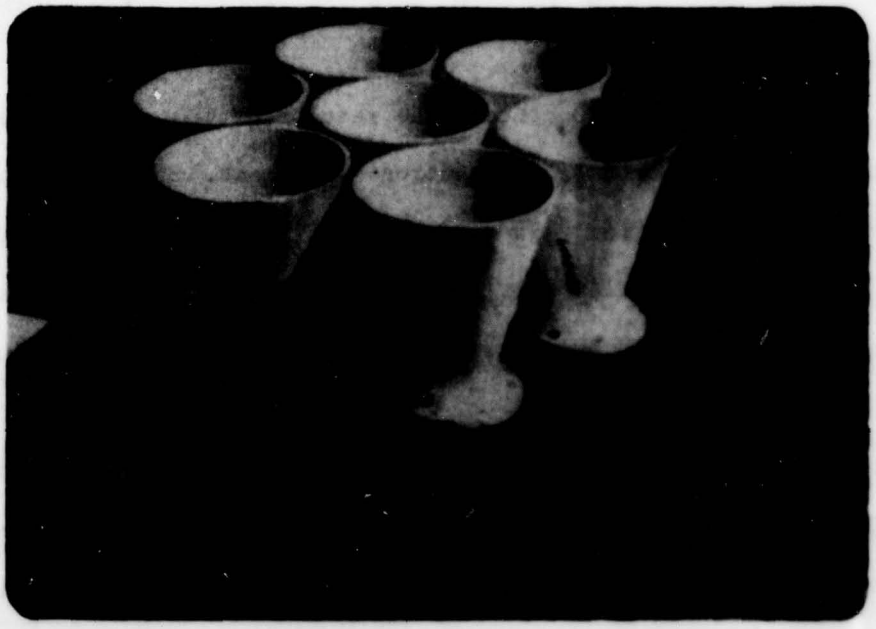

FIGURE B-1
ACOUSTIC ARRAY USED FOR WEAK-WAVE PROPAGATION

Taken from Ref. 28

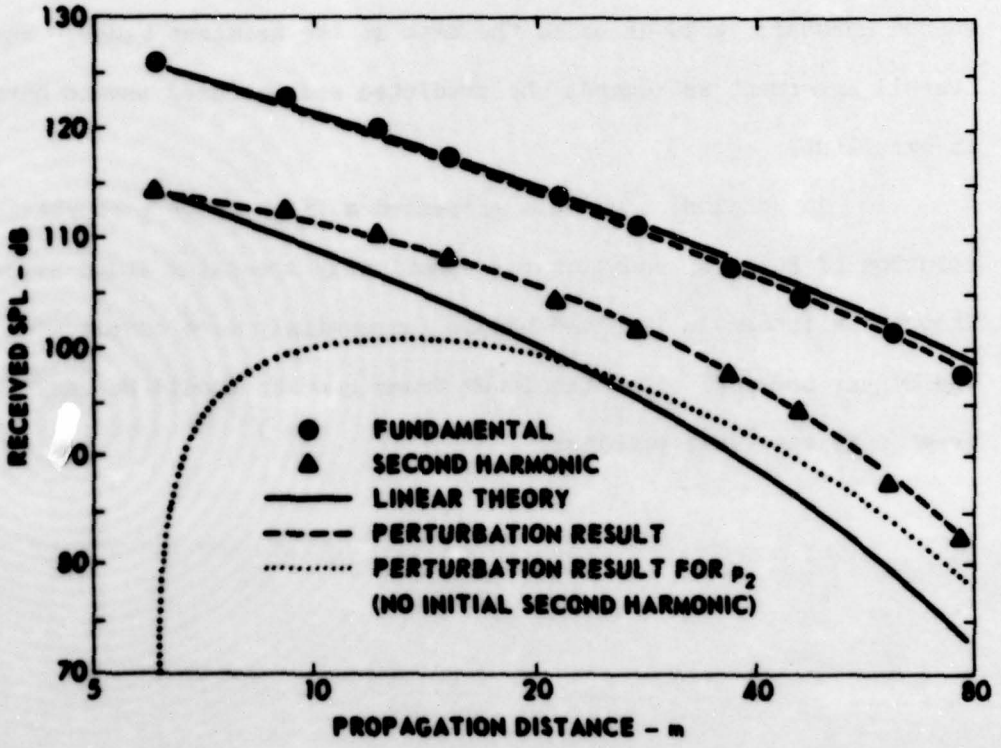

FIGURE B-2
COMPARISON OF PERTURBATION RESULTS WITH PROPAGATION DATA

is zero, the correct second order perturbation result (dashed curve) for p_2 is the arithmetic sum of the dotted curve and the lower solid curve. The need for taking account of the initial second harmonic distortion is well illustrated. It is also interesting that although the fundamental is well described by linear theory, the linear theory prediction for the second harmonic is 10 dB below the data at the greatest range. The overall agreement as regards the predicted and measured second harmonic is excellent.

In conclusion we have presented a fifth order perturbation solution of Burgers' equation for spherically spreading sound waves. Though the integrals involved become increasingly more complicated for the higher order results, the lower order results should be useful for a great many weak-wave problems.

APPENDIX C

SOLUTION OF THE RUDNICK EQUATION FOR SPHERICAL WAVES

Blackstock[34] suggested a spherical wave version of the Rudnick decay rate equation (Eq. 3-7). By analogy with the plane wave case, Blackstock assumed that the decay rate dp_1/dr of the fundamental pressure component is the sum of the decay rate due to absorption $(dp_1/dr)_{abs.} = -\alpha p_1$ and the decay rate $(dp_1/dr)_{f.a.}$ of a spherically spreading sound wave of finite amplitude. The latter decay rate may be found as follows. Let the boundary condition be

$$p_1(r_o,t) = p_{10} \sin \omega t \quad . \tag{C-1}$$

The value of p_1 in the sawtooth region ($\sigma \geq 3$) in the absence of absorption is

$$p_1 = \frac{r_o}{r} \frac{2p_{10}}{1+\sigma} \quad . \tag{C-2}$$

The decay rate $(dp_1/dr)_{f.a.}$ is, from Eq. C-2,

$$\left(\frac{dp_1}{dr}\right)_{f.a.} = \frac{r_o}{r^2} \frac{2p_{10}}{1+\sigma} - \frac{\beta\epsilon k r_o^2}{r^2} \frac{2p_{10}}{(1+\sigma)^2} \tag{C-3}$$

$$= -\frac{1}{r} p_1 - \frac{\beta\epsilon k}{2p_{10}} p_1^2 \quad .$$

By supposition the total decay rate dp_1/dr is then

$$\left(\frac{dp_1}{dr}\right) = \left(\frac{dp_1}{dr}\right)_{abs.} + \left(\frac{dp_1}{dr}\right)_{f.a.}$$

$$= -\alpha p_1 - \frac{1}{r} p_1 - \frac{\beta\epsilon k}{2p_{10}} p_1^2 \quad . \tag{C-4}$$

We now wish to solve Eq. C-4 subject to the condition that the solution reduces to the weak shock solution (Eq. C-2) as $\alpha \to 0$. The form of the solution for the plane wave case (Eq. 3-11) suggests that we try a solution of the form

$$p_1 = \frac{r_o}{r} \frac{A\, e^{-\alpha(r-r_o)}}{1 + f(r)} \quad , \tag{C-5}$$

where A is a constant and the function f(r) is to be determined. Substitution of Eq. C-5 into Eq. C-4 leads to the following form of f(r):

$$f(r) = \frac{A\, \beta\epsilon k r_o}{2p_{10}} e^{\alpha r_o} \int_{\alpha r_o}^{\alpha r} \frac{e^{-\lambda}}{\lambda} d\lambda \quad . \tag{C-6}$$

As in the plane wave case, the choice of $A = 2p_{10}$ yields the weak-shock solution, Eq. C-2, as $\alpha \to 0$. The definition of the exponential integral $E_1(a)$ (see, for example, Ref. 35),

$$E_1(a) = \int_a^\infty \frac{e^{-\lambda}}{\lambda} d\lambda \quad ,$$

may be used to write the expression for f(r) as follows:

$$f(r) = \beta\epsilon k r_o e^{\alpha r_o} \left[E_1(\alpha r_o) - E_1(\alpha r)\right] \quad . \tag{C-7}$$

The expression for p_1, found from Eqs. C-5 and C-7, is

$$p_1 = \frac{r_o}{r} \frac{2p_{10}\, e^{-\alpha(r-r_o)}}{1 + \beta\epsilon kr_o\, e^{\alpha r_o}[E_1(\alpha r_o) - E_1(\alpha r)]} \quad . \tag{C-8}$$

Equation C-8 is simple to evaluate in practice. The exponential integral $E_1(\alpha r)$ may be read from tables or evaluated by certain series representations. See, for example, Ref. 35. Indeed, in the range $0 \leq \alpha r \leq 1$ the series representation for $E_1(\alpha r)$ may be written as[35]

$$E_1(\alpha r) = -\ln(\alpha r) + \sum_{i=0}^{5} a_i (\alpha r)^i \quad , \tag{C-9}$$

with a maximum percentage error of 9×10^{-5}.

The proposed solution (Eq. C-8) was compared to freefield propagation data taken using a siren operating at 6.1 kHz in air. Two views of the siren are shown in Fig. C-1. The 20 circular ports in view b are the sound sources. The siren operates by periodically interrupting the air flow through the ports by means of a motor-driven titanium steel rotor located just behind the ports. For further details see Ref. 28. Because of the relatively high acoustic power output of the siren (approximately 600 W of acoustic power with a 40° beamwidth between the 3 dB down points), the characteristic sawtooth wave shape was already in evidence at a propagation distance of approximately 2 m. Our measured boundary condition was, therefore, a sawtooth wave at a given distance r_m from the source. To use Eq. C-8 we must compute from our measured data the amplitude p_{10} and effective source radius r_o of a sinusoid which would yield the measured sawtooth wave at range r_m. This is easily

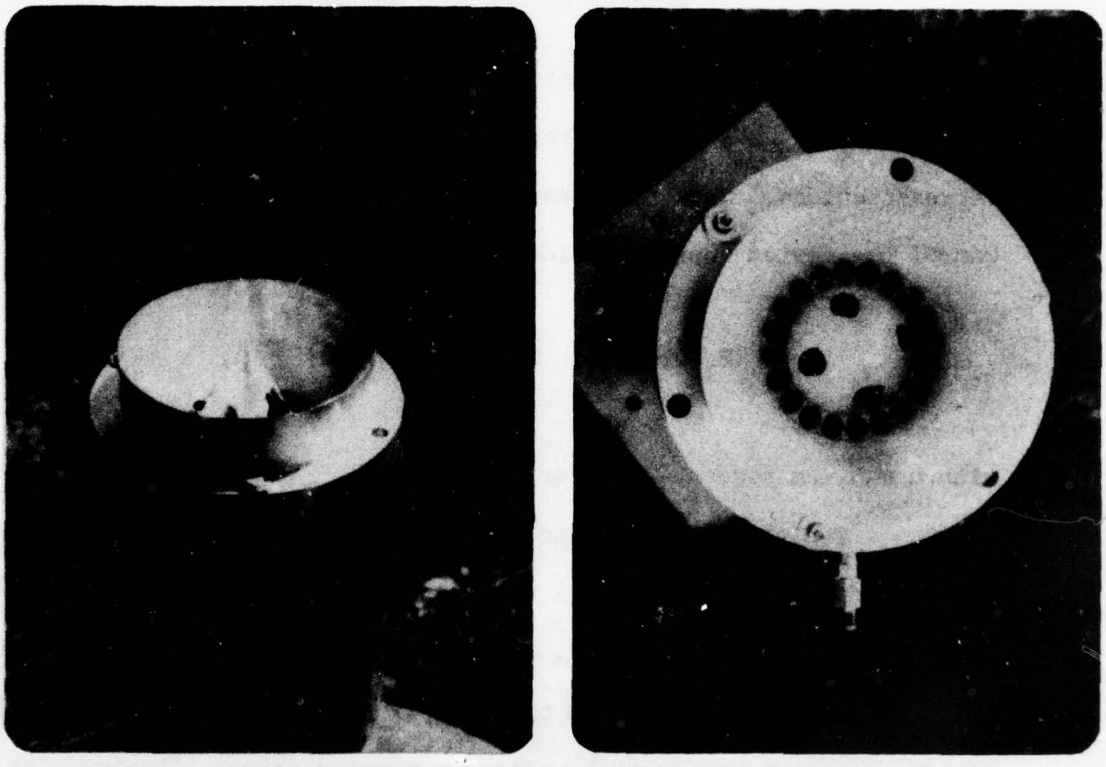

a b

FIGURE C-1
ACOUSTIC SIREN USED IN THE
STRONG-WAVE EXPERIMENT
(a: SIDE VIEW, b: VIEW FROM ABOVE THE SIREN)

Taken from Ref. 28

AD-A035 694 TEXAS UNIV AT AUSTIN APPLIED RESEARCH LABS F/G 20/1
SATURATION OF PLANE ACOUSTIC WAVES AND NOTES ON THE PROPAGATION--ETC(U)
JAN 77 D A WEBSTER F44620-76-C-0040
UNCLASSIFIED ARL-TR-77-4 AFOSR-TR-77-0065 NL

2 OF 2
AD A035694

END
DATE FILMED
3-77

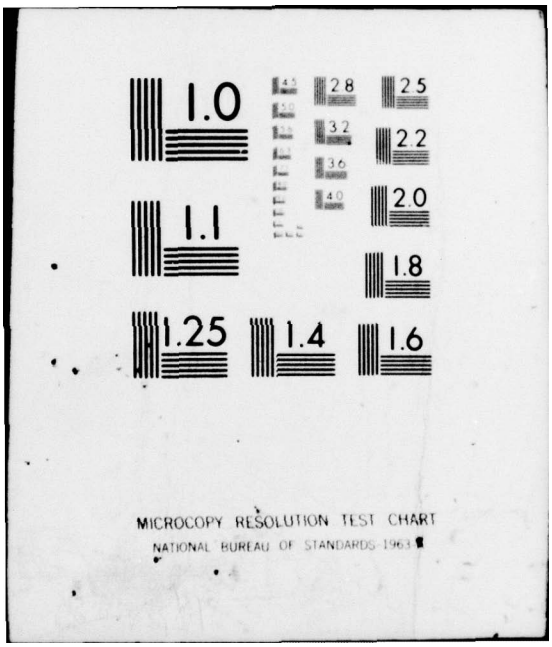
1.0
1.1
1.25
1.4
1.6
2.8
3.2
3.6
4.0
2.5
2.2
2.0
1.8
MICROCOPY RESOLUTION TEST CHART
NATIONAL BUREAU OF STANDARDS 1963

accomplished by using the sawtooth solution (Eq. C-2). Let p_{1m} be the measured value of the fundamental pressure component at range r_m. Then, using Eq. C-2, we have

$$p_{1m} = \frac{r_o}{r} \frac{2p_{10}}{1+\sigma} \Bigg|_{\substack{\sigma = 3 \\ r=r_m}} , \qquad (C\text{-}10)$$

and

$$\sigma = \frac{\beta p_{10} k r_o}{\rho_o c_o^2} \ln\left(\frac{r_m}{r_o}\right) = 3 . \qquad (C\text{-}11)$$

Equations C-10 and C-11 may be solved for p_{10} and r_o, since all other quantities are known.

Figure C-2 shows the results of a comparison of Eq. C-8 with the measured data. The value of the absorption coefficient α was found to be 0.0059 Np/m from a small-signal experiment under similar conditions and is also consistent with the computed value from Ref. 36. The values of p_{1m} and r_m were 2.29×10^3 μbar and 2.19 m, respectively. The values of p_{10} and r_o computed from Eq. C-10 were, respectively, 1.1×10^5 μbar and 0.09 m. The solid curve is the linear theory prediction; the dashed curve represents the solution of the "Rudnick model" equation. The latter is seen to provide a good fit to the data.

In summary the model proposed here, although ad hoc, does seem to provide a good description of the experimental data. Further experimental verification of this model may be found in Ref. 28. The model should be useful in a number of spherical wave problems, though its use is restricted to strong waves.

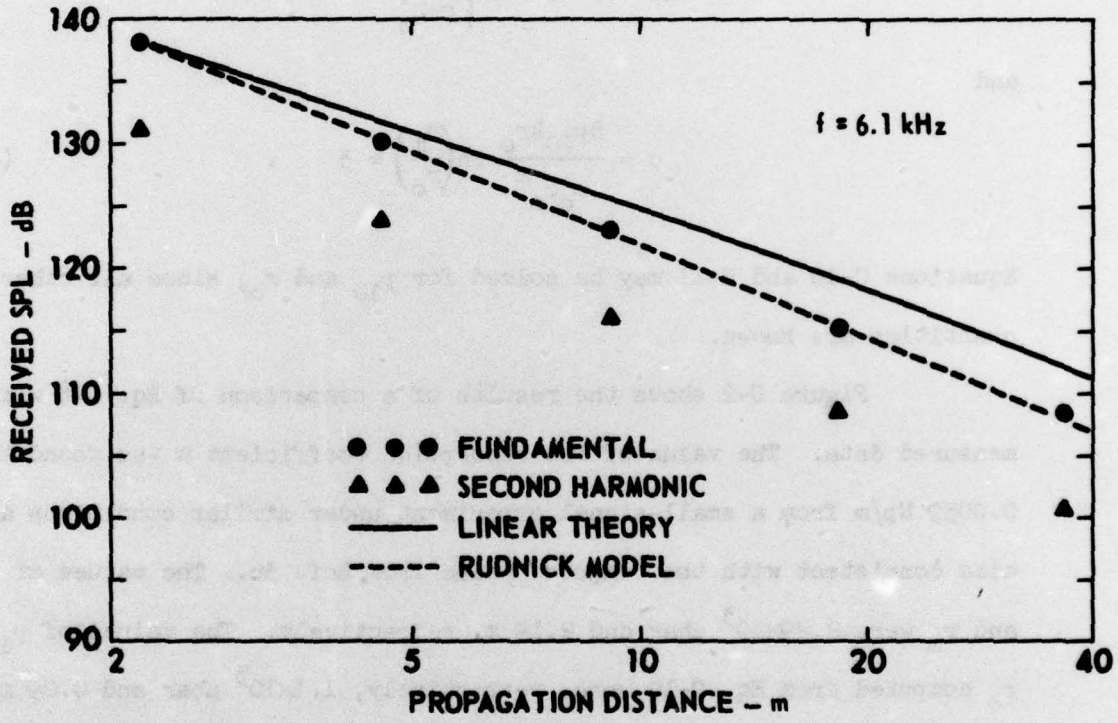

FIGURE C-2
COMPARISON OF THE RUDNICK MODEL
WITH PROPAGATION DATA

REFERENCES

1. D. T. Blackstock, "Nonlinear Acoustics (Theoretical)," in Amer. Inst. Phys. Handbook, 3rd Edition, D. Gray, ed. (McGraw-Hill Book Co., Inc., New York, 1972).
2. C. H. Allen, "Finite Amplitude Distortion in a Spherically Diverging Sound Wave in Air," Ph.D. Dissertation, The Pennsylvania State University (1950). Much of this work also appears in "Atmospheric Physics and Sound Propagation," Final Report by Acoustics Laboratory, The Pennsylvania State University, under Signal Corps Contract W36-039-SC-32001 (September 1950) (ATI 94971).
3. J. A. Shooter, T. G. Muir, and D. T. Blackstock, "Acoustic Saturation of Spherical Waves in Water," J. Acoust. Soc. Am. 55, 55-62 (1974).
4. W. W. Lester, "Experimental Study of the Fundamental-Frequency Component of a Plane, Finite-Amplitude Wave," J. Acoust. Soc. Am. 34, 1991(A) (1962); 40, 847-851 (1966).
5. I. Rudnick, "Measurement of the Attenuation of a Repeated Shock Wave," Technical Report No. 3, Soundrive Engine Company, Los Angeles, California (1953).
6. H. Medwin, "Attenuation of Guided, Repeated Shock Waves in Gases," J. Acoust. Soc. Am. 36, 870-877 (1964).
7. S. H. Burns, "Finite-Amplitude Distortion in Air at High Acoustic Pressures," J. Acoust. Soc. Am. 41, 1157-1169 (1966).

8. F. M. Pestorius, "Propagation of Plane Acoustic Noise of Finite Amplitude," Ph.D. Dissertation, The University of Texas at Austin; also Technical Report No. 23 (ARL-TR-73-23), Applied Research Laboratories, The University of Texas at Austin (August 1973). (AD 778 868)

9. D. F. Pernet and R. C. Payne, "Non-Linear Propagation of Signals in Air," J. Sound. Vib. 17, 383-396 (1971).

10. S. D. Poisson, "Memoire sur la Theorie du Son," J. E'cole Polytech. (Paris) 7, 319-370 (1808).

11. J. Challis, "On The Velocity of Sound," Phil. Mag. 32 (Series 3), 494-499 (1848).

12. D. T. Blackstock, "Connection Between The Fay and Fubini Solutions for Plane Sound Waves of Finite Amplitude," J. Acoust. Soc. Am. 39, 1019-1026 (1966).

13. G. Kirchhoff, "Uber der Einfluss der Warmeleitungs in Gase auf die Schallbewegung," Ann. Physik 134, 177-193 (1868).

14. H. Lamb, Hydrodynamics (Dover Publications, New York, 1945), pp. 619-622.

15. M. E. Schaeffer, "The Suppression of Sound with Sound," Thesis, The University of Texas at Austin; also, Technical Report No. 75-64 (ARL-TR-75-64), Applied Research Laboratories, The University of Texas at Austin (1975). (ADA 023128)

16. J. L. McKittrick, D. T. Blackstock, and W. M. Wright, "Profile of Repeated Shock Waves in a Tube," J. Acoust. Soc. Am. 42, 1153(A) (1967).

17. M. J. Lighthill, in Surveys in Mechanics (Cambridge University Press, Cambridge, England, 1956), pp. 250-351.

18. J. S. Mendousse, "Nonlinear Dissipative Distortion of Progressive Sound Waves at Moderate Amplitudes," J. Acoust. Soc. Am. 25, 51-54 (1953).

19. D. T. Blackstock (1976), Personal Communication.

20. A. B. Coppens and J. V. Sanders, "Finite-Amplitude Standing Waves in Rigid-Walled Ducts: Behavior for Strengths Precluding Shock Formation," J. Acoust. Soc. Am. 43, 516-529 (1968).

21. H. M. Merklinger, "Fundamental-Frequency Component of a Finite-Amplitude Plane Wave," J. Acoust. Soc. Am. 54, 1760-1761(L) (1973).

22. P. J. Westervelt, "Self Scattering of High Intensity Sound," in Proceedings of the Third International Congress on Acoustics, Stuttgart 1959 (Elsevier, Amsterdam, 1961), Vol. 1, pp. 316-321.

23. A. L. Thuras, R. T. Jenkins, and H. T. O'Neil, "Extraneous Frequencies Generated in Air Carrying Intense Sound Waves," J. Acoust. Soc. Am. 6, 173-180 (1935).

24. I. Rudnick, "Theory of The Attenuation of Very High Amplitude Sound Waves," Technical Report No. 1, Soundrive Engine Company, Los Angeles, California (1952).

25. S. H. Burns, "Rational Design of Matched Absorbing Terminations for Tubes," J. Acoust. Soc. Am. 34, 306-318 (1971).

26. D. A. Webster and D. T. Blackstock, "Finite-Amplitude Saturation of Plane Sound Waves in Air," Paper presented at 91st Meeting of The Acoustical Society of America, Washington, D.C. (1976).

27. M. A. Theobald, D. A. Webster, and D. T. Blackstock, "The Importance of Finite-Amplitude Distortion in Outdoor Propagation Experiments," Paper presented at the 7th International Symposium on Nonlinear Acoustics, Blacksburg, Virginia (1976).

28. M. A. Theobald, "Experimental Study of Outdoor Propagation of Spherically Spreading Periodic Acoustic Waves of Finite Amplitude," Master's Thesis in Mechanical Engineering, to be published 20 January 1977, The University of Texas at Austin, Austin, Texas; also Applied Research Laboratories Technical Report No. 77-5 (ARL-TR-77-5), Applied Research Laboratories, The University of Texas at Austin.

29. H. M. Merklinger, R. H. Mellen, and M. B. Moffett, "Finite Amplitude Losses in Spherical Sound Waves," J. Acoust. Soc. Am. 59, 755-759 (1976).

30. J. C. Lockwood, T. G. Muir, and D. T. Blackstock, "Directive Harmonic Generation in the Radiation Field of a Circular Piston," J. Acoust. Soc. Am. 53, 1148-1153 (1973).

31. K. A. Naugol'nykh, "Propagation of Spherical Sound Waves of Finite Amplitude in a Viscous, Heat-Conducting Medium," Sov. Phys. Acoust. 5, 79-84 (1959).

32. M. H. Safar, "The Propagation of Spherical Acoustic Waves of Finite Amplitude in Fresh and Sea Water," J. Sound Vib. 13, 1-7 (1970).

33. D. T. Blackstock and J. G. Willette, "The Effect of Nonlinear Propagation Distortion on High-Power, Low-Frequency Sonars" (U), Technical Report No. 71-11 (ARL-TR-71-11), Applied Research Laboratories, The University of Texas at Austin (29 March 1971), Appendix. (CONFIDENTIAL)

34. D. T. Blackstock (1975), Personal Communication.

35. M. Abramowitz and I. Stegun, Handbook of Mathematical Functions, National Bureau of Standards Applied Mathematics Series 55, Government Printing Office (1964).

36. H. E. Bass, "Study of Sound Propagation in Air," Thesis, Department of Physics, The University of Mississippi, University, Mississippi; also, Final Technical Report for U.S. Army Research Office Contract 1123-E (1976).

3 January 1977

DISTRIBUTION LIST FOR
ARL-TR-77-4
UNDER GRANT 04-5-022-12, CONTRACT F44620-76-C-0040, and
CONTRACT NAS1-14160
UNCLASSIFIED

AFOSR/NA (16)
Bldg. 410
Attn: LTC L. W. Ormand
Bolling, AFB, DC 20332

U. S. Department of Commerce (20)
National Oceanic and Atmospheric
Administration
Environmental Research Laboratories
Attn: Freeman Hall
Boulder, CO 80302

NASA Langley Research Center (3)
Acoustics and Noise Reduction Division
Attn: J. M. Seiner, Mail Stop 460
Hampton, VA 23365

Brown University
Department of Physics
Attn: R. T. Beyer (1)
P. J. Westervelt (1)
Providence, RI 02912

Georgia Institute of Technology (1)
School of Mechanical Engineering
Attn: A. D. Pierce
Atlanta, GA 30332

Hendrix College (1)
Department of Physics
Attn: R. L. Rolleigh
Conway, AR 72032

Kalamazoo College (1)
Department of Physics
Attn: W. M. Wright
Kalamazoo, MI 49008

Naval Postgraduate School
Physics and Chemistry Department
Attn: A. B. Coppens (1)
J. V. Sanders (1)
Monterey, CA 93940

Naval Research Laboratory (1)
Underwater Sound Reference Division
Attn: P. H. Rogers
P. O. Box 8337
Orlando, FL 32806

Naval Underwater Systems Center
New London Laboratory
Attn: M. B. Moffett (1)
W. L. Konrad (1)
R. H. Mellen (1)
New London, CT 06320

Office of Naval Research
Code 222
Attn: R. F. Obrochta (1)
800 North Quincy Street
Arlington, VA 22217

Pennsylvania State University (1)
Applied Research Laboratory
Attn: F. H. Fenlon
P. O. Box 30
State College, PA 16801

Raytheon Company (1)
Attn: J. C. Lockwood
W. Main Road
Portsmouth, RI 02871

University of Tennessee (1)
Department of Physics
Attn: M. A. Breazeale
Knoxville, TN 37916

Cambridge University (1)
University Engineering Department
Attn: J. E. Ffowcs-Williams
Trumpington Street
Cambridge CB 2 1PZ
ENGLAND

Dist. List for ARL-TR-77-4 under Grant 04-5-022-12, Contract F44620-76-C-0040, and Contract NAS1-14160 (cont'd)

Defence Research Establishment Atlantic (1)
Attn: H. M. Merklinger
P. O. Box 1012
Dartmouth, Nova Scotia
CANADA

Technical University of Denmark (1)
Fluid Mechanics Department
Attn: L. Bjørnø
Building 404
DK-2800 Lyngby
DENMARK

University of Birmingham (1)
Electronic and Electrical
Engineering Department
Attn: H. O. Berktay
P. O. Box 36 B
Birmingham B15 2TT
ENGLAND

Naval Research Laboratory
Code 8151: Attn: A. L. Van Buren (1)
Code 8120: Attn: A. I. Eller (1)
Washington, DC 20375

The Clayton H. Allen Corporation (1)
651 Concord Avenue
Attn: Dr. Clayton H. Allen
Cambridge, MA 02138

Paul S. Veneklasen and Associates (1)
1711 Sixteenth Street
Attn: Mark E. Schaffer
Santa Monica, CA 90404

A & B Science Consultants, Inc. (1)
P.O. Box 443
Attn: Henry E. Bass, President
University, MS 38677

Stanford University (1)
Department of Aeronautics &
Astronautics
Attn: K. Karamcheti
Stanford, CA 94305

Applied Physics Department (1)
Royal Melbourne Institute of Technology
124 La Trobe Street
Attn: John D. Buntine
Melbourne, Victoria, 3000, AUSTRALIA

Yale University (1)
Mason Laboratory M4
Attn: R. E. Apfel
New Haven, CT 06511

USAFA (Library) (1)
USAFA, CO 80840

AFIT Library (AU) (1)
AFIT, Area B, Bldg. 640
Wright-Patterson AFB, OH 45433

NASA Langley Research Center (1)
Attn: Library
Hampton, VA 23365

Office of Naval Research (1)
Physics Program Office (Code 421)
Attn: L. E. Hargrove
800 N. Quincy Street
Arlington, VA 22217

AFAPL (1)
Attn: Paul Shahady
Wright-Patterson AFB, OH 45433

Aeronautical Research Associates of (1)
Princeton, Inc.
50 Washington Road
Princeton, NJ 08450

Case Western University (1)
School of Engineering
Attn: Prof. Greber
University Circle
Cleveland, OH 44106

Near, Inc. (1)
510 Clyde Avenue
Mountain View, CA 94043

Dist. List for ARL-TR-77-4 under Grant 04-5-022-12, Contract F44620-76-C-0040, and Contract NAS1-14160 (cont'd)

University of Southern California (1)
Department of Aerospace Engineering
Attn: Dr. Ho, Chih-Ming
University Park
Los Angeles, CA 90007

University of Toronto
Institute of Aerospace Studies
Attn: H. S. Ribner (1)
I. I. Glass (1)
4925 Dufferin Street
Downsview, Ontario
Toronto, Canada, M3H 5T6

University of Leeds (1)
Department of Mathematics
Leeds, England
Attn: David G. Crighton

(1)

M.I.T.
Ocean Engineering Department
Cambridge, MA 02139
Attn: W. L. Harris

Virginia Polytechnic Institute and State University
Department of Engineering Science and Mechanics
Blacksburg, VA 24061
Attn: John Kaiser (1)
Ali Nayfeh (1)

Purdue University
Lafayette, IN 47907
Attn: C. Paul Kentzer (1)
P. G. Vaidya (1)

University of California
Los Angeles, CA 90024
Attn: Isadore Rudnick (1)

University of Göttingen
42-44 Burger Ctr.
Göttingen, Germany
Attn: M. R. Schroeder (1)

University of Toronto
Toronto, Ontario, Canada
Attn: David S. Scott (1)

Bell Laboratories
Holmdel, NJ 07722
Attn: Robert N. Thurston (1)

Institute of Sound and Vibration Research
The University
Attn: Dr. C. L. Morfey (1)
Southampton SO9 5NH
ENGLAND